Universidade Federal do Ceará
Centro de Tecnologia
Departamento de Engenharia de Teleinformática
Programa de Graduação em Engenharia de Telecomunicações

KENNETH BRENNER DOS ANJOS BENÍCIO

CHANNEL ESTIMATION AND JOINT BEAMFORMING DESIGN FOR MULTI-IRS MIMO SYSTEMS

FORTALEZA – CE
2021

KENNETH BRENNER DOS ANJOS BENÍCIO

CHANNEL ESTIMATION AND JOINT BEAMFORMING DESIGN FOR MULTI-IRS MIMO SYSTEMS

Trabalho de Conclusão de Curso submetido à Coordenação do Programa de Graduação em Engenharia de Telecomunicações da Universidade Federal do Ceará como parte dos requisitos para a obtenção do grau de **Bacharel em Engenharia de Telecomunicações**.
Orientador: Prof. Dr. André Lima Férrer de Almeida.
Co-Orientador: M.Ed Bruno Sokal.

FORTALEZA – CE
2021

KENNETH BRENNER DOS ANJOS BENÍCIO

CHANNEL ESTIMATION AND JOINT BEAMFORMING DESIGN FOR MULTI-IRS MIMO SYSTEMS

Trabalho de Conclusão de Curso submetido à Coordenação do Programa de Graduação em Engenharia de Telecomunicações da Universidade Federal do Ceará como parte dos requisitos para a obtenção do grau de **Bacharel em Engenharia de Telecomunicações**.

Aprovada em: ____/____/_____.

BANCA EXAMINADORA

Prof. Dr. André Lima Férrer de Almeida (Orientador)
Universidade Federal do Ceará (UFC)

M.Ed Bruno Sokal (Coorientador)
Grupo de Pesquisa em Telecomunicações sem Fio (GTEL)

Prof. Dr. Walter Freitas Jr.
Universidade Federal do Ceará (UFC)

Prof. Dr. Yuri Carvalho Barbosa Silva
Universidade Federal do Ceará (UFC)

Dedico este trabalho ao meu avô José Chagas Ferreira que infelizmente não tive a oportunidade de conviver por um longo período, mas que até tenho lembro carinhosamente da companhia.

AGRADECIMENTOS

Aos meus pais, Jacqueline Silva dos Anjos Benício e José Ribamar Benício Ferreira, pelo apoio imprescindível ao longo dos anos, pois sem a tranquilidade e segurança fornecidas jamais seria possível chegar até o fim dessa etapa.

À minha avó, Joventina Benício de Freitas, pela presença, pelas conversas e pelo carinho ao longo de toda minha vida. Espero poder continuar convivendo com tua presença por muitos anos.

Aos professores que ao longo dessa jornada estimularam a busca pelo conhecimento como uma forma de compreender o mundo, resultando em minha paixão pela pesquisa acadêmica.

Aos meus orientadores, prof. André e Bruno, pelas valiosas discussões, pela paciência e pelo imensurável aprendizado fornecido ao longo de todo o período que já trabalhamos juntos.

Aos contemporâneos do Departamento de Engenharia de Teleinformática(DETI) e aos meus amigos pessoais que tanto me ajudaram, indireta ou diretamente, ao longo da graduação. Pelas produtivas discussões que me fizeram crescer como indivíduo e pela presença nos momentos mais dificeis, serei eternamente grato. Sou particularmente grato ao Arthur Anderson, ao Artur Martins e ao Daniel Alves pelo fortissimo apoio nos momentos de maiores dificuldades ao longo dessa reta final.

Não menos importante, sou demasiadamente grato pelas muitas conversas e conselhos do meu querido amigo Endley Fernando que infelizmente deixou a todos cedo demais.

"If I have seen further than others, it is by standing upon the shoulders of giants."

Isaac Newton (1675)

RESUMO

Neste trabalho, propomos um procedimento para a formatação conjunta de feixe e a estimação de canal para sistemas MIMO assistidos por múltiplas IRSs. Investigamos o cenário no qual várias IRSs estão localizadas no local exato dos espalhadores naturais do canal. Ademais, também investigamos a eficiência espectral, os benefícios e as desvantagens de implantar múltiplas IRSs e traçamos comparações entre cenários com uma única IRS ou nenhuma IRS. Nossos resultados computacionais mostram uma compensação entre o número de elementos refletivos e o número total de IRSs no sistema.

Keywords: Interfaces Refletoras Inteligentes, Sistemas MIMO, Estimação de Canal, Formatação de Feixe.

ABSTRACT

In this work, we propose a channel estimation and joint beamforming design method for multi-IRS MIMO systems. We investigate the scenario where multiple IRSs are located on the exact spot of the channel scatterers. We investigate the spectral efficiency, benefits and drawbacks of deploying multiple IRSs in comparison with a scenario with a single or no IRS. Our simulation results show a trade-off between the number of reflecting elements and the total number of IRSs in the system.

Keywords: Intelligent Reflecting Surfaces, MIMO Systems, Channel Estimation, Beamforming Design.

LIST OF FIGURES

LIST OF ACRONYMS

6G	Sixth Generation
AoA	Angle of Arrival
AoD	Angle of Departure
AWGN	Additive White Gaussian Noise
B5G	Beyond Fifth Generation
BPSK	Binary Phase-Shift Keying
CSI	Channel State Information
DFT	Discrete Fourier Transform
EE	Energy Efficiency
FD	Full-Duplex
HD	Half-Duplex
IRS	Intelligent Reflective Surface
LoS	Line-of-Sight
LS	Least Squares
MIMO	Multiple Input Multiple Output
mmWave	Millimeter Wave
NLoS	No Line-of-Sight
PA	Perfect Absorbers
PIN	Positive-Intrinsic-Negative
QPSK	Quadrature Phase-Shift Keying
RF	Radio Frequency
RS	Regular Scatterers
RX	Receiver
SE	Spectral Efficiency
SINR	Signal-to-Interference-plus-Noise Ratio
SISO	Single Input Single Output
SNR	Signal-to-Noise Ratio
SVD	Single Value Decomposition
TX	Transmitter
ULA	Uniform Linear Array
URA	Uniform Rectangular Array

LIST OF SYMBOLS

$(\cdot)^*$	Conjugate
$(\cdot)^+$	Moore-Penrose pseudo-inverse
$(\cdot)^{\mathrm{H}}$	Hermitian
$(\cdot)^{\mathrm{T}}$	Transpose
$\diamond$	Khatri-Rao Product
$\odot$	Hadamard Product
$\oslash$	Element-wise division
$\otimes$	Kronecker Product
$\mathbf{X}$	Represents matrix
$\mathbf{x}$	Represents vector
x	Represents scalar

CONTENTS

1 Introduction

Intelligent Reflective Surface (IRS) have caught the attention of the wireless communications community in recent years (GONG et al., 2020; LIASKOS et al., 2018), for being a promising candidate for Beyond Fifth Generation (B5G) and the Sixth Generation (6G) wireless networks. An IRS is a 2D-panel (BUKHARI et al., 2019) composed of N (semi-) passive reflecting elements that apply phase-shifts to the the impinging electromagnetic waves so that they add constructively or destructively at the intended receiver, improving the overall Signal-to-Noise Ratio (SNR) in the system. Typically the only active element in the IRS structure is the smart controller, which has a negligible power consumption compared to other current technologies such as relays (WU; ZHANG, et al., 2021). However, there's known schemes of relaying using IRS where some elements within the surface are consider to be active to account for the lack of Radio Frequency (RF) chains from the IRS (TAHA et al., 2021). These elements act like sensors to the IRS collecting information that will be later used to aid in the estimation of the channel parameters at the IRS, since it needs an accurate estimation to correctly optimize the reflection of its elements.

One of the main reasons the IRS theme has attracted such attention in recent years is that, depending on the number of reflecting elements and its phase-shift design, the SNR gain grows quadratically. The limits of this gain are discussed in (BJÖRNSON et al., 2019), where the authors analyze how large an IRS must be, i.e., how many reflecting elements are required to surpass the known relaying schemes.

In the work of (WANG, P. et al., 2020) IRSs are used to diminish the impact of coverage holes in Millimeter Wave (mmWave) Multiple Input Multiple Output (MIMO) systems. It is shown that by creating an effective virtual Line-of-Sight (LoS) path between the transmitter and the receiver, the IRS can be used to minimize the effects of severe path loss and the high directivity intrinsic to mmWave communications. Nonetheless, since the IRS is a recent concept, the authors of (ÖZDOGAN et al., 2019; BJÖRNSON et al., 2020) explore the physical laws of the IRS while dispelling some myths surrounding the community.

Along with a new concept comes the technical difficulties to bring it to life. As extensively discussed in (WU; ZHANG, et al., 2021), at the present there's important topics surrounding the IRS that are still in need of further research by the wireless communication community, e.g., the physical-layer security (SHEN et al., 2019) and the establishment of a standard transmission protocol (YANG et al., 2020) in the context of IRS-aided systems. However, these particular topics are out of the scope of the present work, but can be worked on in the future.

1.1 Related Works and Contributions

Although an IRS can offer a very high SNR gain at low energy consumption levels compared to other technologies, even with some active elements within the surface, one of the main problems is that of Channel State Information (CSI) acquisition. Since the IRS is usually a fully passive structure with no digital signal processing capability, channel estimation must be performed at the receiver using pilots sent by the transmitter and reflected by the IRS according to predefined patterns. Recent works in the literature have proposed solutions that address this problem such as (ARAÚJO et al., 2021), (WEI et al., 2021), (ARDAH et al., 2021) and (WANG, Z. et al., 2020).

Closely related to the this paper are the works of channel estimation protocols from

(ARAÚJO et al., 2021; WEI et al., 2021) and the joint beamforming design from (JENSEN; DE CARVALHO, 2020; ZAPPONE et al., 2020). The authors in (ARAÚJO et al., 2021) propose a tensor modeling approach to obtain the CSI using a supervised method, where two algorithms were formulated to decouple the estimation of the involved channels. The work in (WEI et al., 2021) also presents a tensor-based approach for channel estimation, where the authors propose three different algorithms. Therein, the authors also discuss the beamforming problem. In (JENSEN; DE CARVALHO, 2020), an optimal channel estimation scheme guided by the minimum variance unbiased estimator is proposed. In (ZAPPONE et al., 2020), the authors discuss different channel estimation algorithms as well as joint IRS phase-shift optimization and active beamforming designs for MIMO systems assisted by a single IRS.

In this work, we consider a MIMO communication system assisted by multiple IRSs. Assuming a specular multipath propagation scenario, we place multiple IRSs on the exact spot of the dominant scatterers. We propose one channel estimation protocol and a joint passive (IRSs elements phase-shifts) and active (transmitter/receiver) beamformings methods for this scenario. We investigate the possible benefits and drawbacks of the proposed multi-IRS system model, in comparison with a scenario with a single or no IRS. In particular, assuming a fixed total number of reflecting elements in the system, we compare a centralized deployment with a single IRS with a distributed one having multiple IRSs. The numerical results show the remarkable Spectral Efficiency (SE) gains of a Multi-IRS MIMO communication system.

The main contributions of this work are summarized as follow:

- We propose a Multi-IRS aided MIMO system scenario and show that it reaches higher SE compared to single-IRS aided MIMO system.
- We provide two pilot-assisted algorithms to obtain the channel estimation for the proposed scenario.
- We offer system design recommendations for the proposed algorithms.

1.2 Organization

The rest of this document is organized into 4 parts, each comprised of a number of sections that will be discussed in their respective chapters:

- Chapter 2: In this chapter, theoretical foundation of this work is discussed. First we explain important concepts about the IRS and its basic practical implementation. Following we obtain the received signal model for the IRS-aided Single Input Single Output (SISO) system and for the IRS-aided MIMO systems.
- Chapter 3: In this chapter, we discuss the system model for the proposed Multi-IRS aided MIMO systems. Then we proposed two methods to obtain the CSI for the proposed scenario considering the IRS as perfect absorbers or as part of the channel interference acting regular scatterers.
- Chapter 4: In this chapter, we obtain and discuss the numerical results for the proposed scenario in the light of the SE.
- Chapter 5: In this chapter, we discuss our conclusions about the proposed scenario and our perspectives of expansion of this work.

The content and scientific contributions present in this study have been partially published with the following bibliographic information

- **K. B. dos A. Benicio**, B. Sokal, A. L. F. de Almeida, "Channel Estimation and Joint Beamforming Design for Multi-IRS MIMO systems", in *Brazilian Symposium on Telecommunications and Signal Processing*, Sep. 2021,pp. 1-5

2 Theoretical Background

This chapter is divided into four main sections. The first section shows the notation and mathematical identities that will be used in this work. The second section will explain the core concept of IRSs from the basics of how we can mathematically model its configurable elements to more technical questions about its architecture and practical limitations that appear when it comes to its implementation. The third section shows the basics of IRS-aided SISO systems and its received signal model. Furthermore, the concept of passive beamforming and power scaling will be discussed. Finally, in the fourth section, we discuss the IRS-aided MIMO systems, starting from core concepts of MIMO systems like capacity, multiplexing and active beamforming.

2.1 Notation and Identities

Scalars and column vectors are represented by lowercase letters $(a, b, \dots)$ and boldface lowercase letters $(\mathbf{a}, \mathbf{b}, \dots)$, respectively. Matrices are symbolized by boldface capital letters $(\mathbf{A}, \mathbf{B}, \dots)$. $\mathbf{X}^*$, $\mathbf{A}^{\mathrm{T}}$, $\mathbf{A}^{\mathrm{H}}$, and $\mathbf{A}^+$ stand for the conjugate, transpose, Hermitian, and Moore-Penrose pseudo-inverse respectively. The jth column of $\mathbf{A} \in \mathbb{C}^{I\times J}$ is denoted by $\mathbf{a}_j \in \mathbb{C}^{I\times 1}$. The nth element of the vector $\mathbf{x} \in \mathbb{C}^{N\times 1}$ is defined as x_n. The operator $\mathrm{vec}(\cdot)$ transforms a matrix into a vector by stacking its columns, e.g., $\mathrm{vec}(\mathbf{A}) = \mathbf{a} \in \mathbb{C}^{IJ\times 1}$, while the $\mathrm{unvec}(\cdot)$ operator does in the inverse operation, i.e., $\mathrm{unvec}_{I\times J}(\mathbf{a}) = \mathbf{A} \in \mathbb{C}^{I\times J}$. The operator $\mathrm{diag}(\cdot)$ converts a vector into a diagonal matrix, $\mathrm{diag}_j(\mathbf{B})$ forms a diagonal matrix of size $R \times R$ out of the jth column of $\mathbf{B} \in \mathbb{C}^{R\times J}$. The operator $||\cdot||$ computes the absolute value of a given element. The $M \times M$ identity matrices is denoted by $\mathbf{I}_M$. The Kronecker product between two matrices is denoted by

$$\mathbf{A} \otimes \mathbf{B} = \begin{bmatrix} a_{1,1}\mathbf{B} & a_{1,2}\mathbf{B} & \cdots & a_{1,J}\mathbf{B} \\ a_{2,1}\mathbf{B} & a_{2,2}\mathbf{B} & \cdots & a_{2,J}\mathbf{B} \\ \vdots & \vdots & \ddots & \vdots \\ a_{I,1}\mathbf{B} & a_{I,2}\mathbf{B} & \cdots & a_{I,J}\mathbf{B} \end{bmatrix} \in \mathbb{C}^{RI\times JJ} \tag{2.1}$$

The column-wise Kronecker product, also known as the Khatri-Rao product, is denoted by

$$\mathbf{A} \diamond \mathbf{B} = \begin{bmatrix} a_{1,1}\mathbf{b}_1 & a_{1,2}\mathbf{b}_2 & \cdots & a_{1,J}\mathbf{b}_J \\ a_{2,1}\mathbf{b}_1 & a_{2,2}\mathbf{b}_2 & \cdots & a_{2,J}\mathbf{b}_J \\ \vdots & \vdots & \ddots & \vdots \\ a_{I,1}\mathbf{b}_1 & a_{I,2}\mathbf{b}_2 & \cdots & a_{I,J}\mathbf{b}_J \end{bmatrix} \in \mathbb{C}^{RI\times J} \tag{2.2}$$

The Hadamard product is denoted by:

$$\mathbf{A} \odot \mathbf{B} = \begin{bmatrix} a_{1,1}b_{1,1} & a_{1,2}b_{1,2} & \cdots & a_{1,J}b_{1,J} \\ a_{2,1}b_{2,1} & a_{2,2}b_{2,2} & \cdots & a_{2,J}b_{2,J} \\ \vdots & \vdots & \ddots & \vdots \\ a_{I,1}b_{I,1} & a_{I,2}b_{I,2} & \cdots & a_{I,J}b_{I,J} \end{bmatrix} \in \mathbb{C}^{I\times J} \tag{2.3}$$

The element-wise division operator is denoted by

$$\mathbf{A} \oslash \mathbf{B} = \begin{bmatrix} a_{1,1}/b_{1,1} & a_{1,2}/b_{1,2} & \cdots & a_{1,J}/b_{1,J} \\ a_{2,1}/b_{2,1} & a_{2,2}/b_{2,2} & \cdots & a_{2,J}/b_{2,J} \\ \vdots & \cdots & \ddots & \vdots \\ a_{I,1}/b_{I,1} & a_{I,2}/b_{I,2} & \cdots & a_{I,J}/b_{I,J} \end{bmatrix} \tag{2.4}$$

If we consider that all matrices have compatible dimensions and $\mathbf{\Lambda} = \text{diag}(\boldsymbol{\lambda})$, then the following identities are true and will be used in chapter 3.

I. Identity between the Khatri-Rao product and vec$(\cdot)$ operator:

$$\text{vec}(\mathbf{A}\mathbf{\Lambda}\mathbf{C}) = (\mathbf{C}^{\text{T}} \diamond \mathbf{A})\boldsymbol{\lambda} \tag{2.5}$$

II. Identity between the Kronecker product and vec$(\cdot)$ operator:

$$\text{vec}(\mathbf{ABC}) = (\mathbf{C}^{\text{T}} \otimes \mathbf{A})\text{vec}(\mathbf{B}) \tag{2.6}$$

III. Identity between Khatri-Rao product and Kronecker product:

$$(\mathbf{AC}) \diamond (\mathbf{BD}) = (\mathbf{A} \otimes \mathbf{B})(\mathbf{C} \diamond \mathbf{D}) \tag{2.7}$$

IV. Linearity of vec$(\cdot)$ operator:

$$\text{vec}(\alpha\mathbf{A} + \beta\mathbf{B}) = \alpha\text{vec}(\mathbf{A}) + \beta\text{vec}(\mathbf{B}) \tag{2.8}$$

2.2 Fading in Wireless Channels

The fading phenomenon is characterized by the variation of transmitted power over distance (GOLDSMITH, 2005). The fading can be classified in two major groups: large-scale and small-scale fading. The large-scale fading occur over large distances due the phenomena of path loss and shadowing and the small-scale fading occur over subwavelength distances (GOLDSMITH, 2005).

The path loss occur by the dissipation of the transmitted power density over some large distance due effects of the channel propagation. In a similar fashion there is also the shadowing phenomenon that occur when the transmitted signal suffers blockage due the presence of obstacles between the transmitter and the receiver. The later is usually proportional to the length of the obstacles (GOLDSMITH, 2005).

When it comes to the small-scale fading it can be classified in two major groups: The multipath fading, that affect the frequency characteristics of the channel, and the Doppler spread fading, that affect the time characteristics of the channel. The multipath fading occurs when the signal reach the receiver only after pass across multiple paths of transmission that will combine its components constructively or destructively (GOLDSMITH, 2005). It can be classified in two minor types: flat fading and frequency selective fading. In the flat fading all the frequencies of the channel are equally affected and in the frequency selective fading the frequencies of the channel are unevenly affected (GOLDSMITH, 2005).

Regarding the fading that occurs in the time characteristics of the channel, the Doppler spread fading, it can be further classified in: fast fading and slow fading. As defined in (TSE; VISWANATH, 2005), the fast fading happens when the coherence time[1] is shorter than some application delay threshold and the slow fading happens when the contrary occurs. There are numerous equations to model each type of fading, but the deep analysis of this matter is something out of scope of this work. In Section 3 we discuss how we choose to model our fading components for the proposed multi-IRS aided MIMO system.

Figure 2.1 Different types of fading in wireless channels.

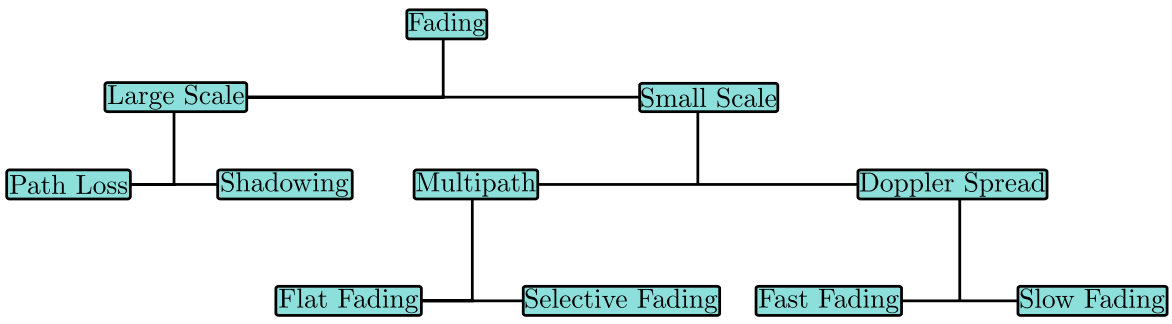

Source: Produced by the author.

[1]The coherence time is defined as the interval over which the impulse response of the channel remains constant (TSE; VISWANATH, 2005).

2.3 IRS Basics

In this section we discuss concepts of an IRS and its practical questions of architecture, hardware and implementation constraints.

2.3.1 What is an IRS?

An IRS is a 2D-panel (BUKHARI et al., 2019) composed of N (semi-) passive reflecting elements that apply phase-shifts to the the impinging electromagnetic waves so that they add constructively or destructively at the intended receiver, improving the overall SNR in the system. From Figure 2.3, we can obtain the phase and amplitude response of the nth element of the IRS by using the expression from (WU; ZHANG, et al., 2021)

$$s_n = \beta_n e^{j\theta_n}. \tag{2.9}$$

The phase-shift, θ_n, and the amplitude, $\beta_n = \{0, 1\} \forall n \in \{1, N\}$ (WU; ZHANG, et al., 2021), represents how the IRS will reflect the incident signal and show to us that the (semi-) IRS can only reflect signals without power amplification. According to Equation (2.9), if we want to turn off an element, it can be done by setting $\beta_n = 0$. However, in practice, there is a coupling between the phase-shift and the amplitude response, θ_n and β_n, respectively, that makes impossible to freely control the phase-shift or the amplitude individually. In this way it is not possible to set β_n to zero (WU; ZHANG, et al., 2021). In Figure 2.2 we show a simplified scheme of how a particular element of the IRS will reflect an incident signal to a intended receiver and also where our reference for the angle θ_n is placed.

Figure 2.2 IRS signal reflection.

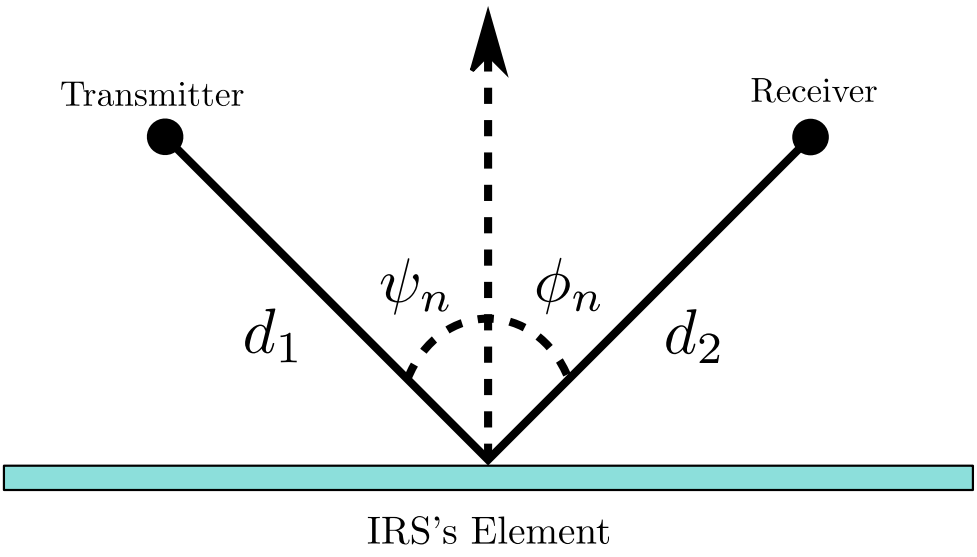

Source: Produced by the author.

Active Elements vs Passive Elements

Typically the only active element in the IRS structure is the smart controller, which has a negligible power consumption compared to other current technologies such as relays (WU; ZHANG, et al., 2021). However, some works are considering to place at the IRS few active elements to perform channel sounding, e.g., (ALEXANDROPOULOS; VLACHOS, 2020) where the IRS is equipped with a single RF chain to actively estimate the channel coefficients. The main differences between these two implementations schemes are:

- Active Elements: The IRS can amplify (at the active elements) and reflect the incoming signals in order to mitigate the path loss and shadowing effects improving the overall SNR of the system. At the same time, the Energy Efficiency (EE) will be lower in this case since the IRS has active elements that increase its power consumption (YOU; ZHANG, 2021).

- Passive Elements: The IRS reflects signals without any kind of amplification or signal processing. Still, because it cannot amplify incident signals the path loss and shadowing are the biggest obstacle to achieve a decent SE or a precise estimation of the CSI. However, (DI RENZO et al., 2020) analyses the EE of a single IRS against relay schemes of Half-Duplex (HD) and Full-Duplex (FD). It is highlighted that an IRS with hundreds of reflective elements can outperforms relay-aided systems in terms of transmission data rate and EE if it is placed at equal distance of the transmitter and the receiver.

Figure 2.3 IRS with a smart controller.

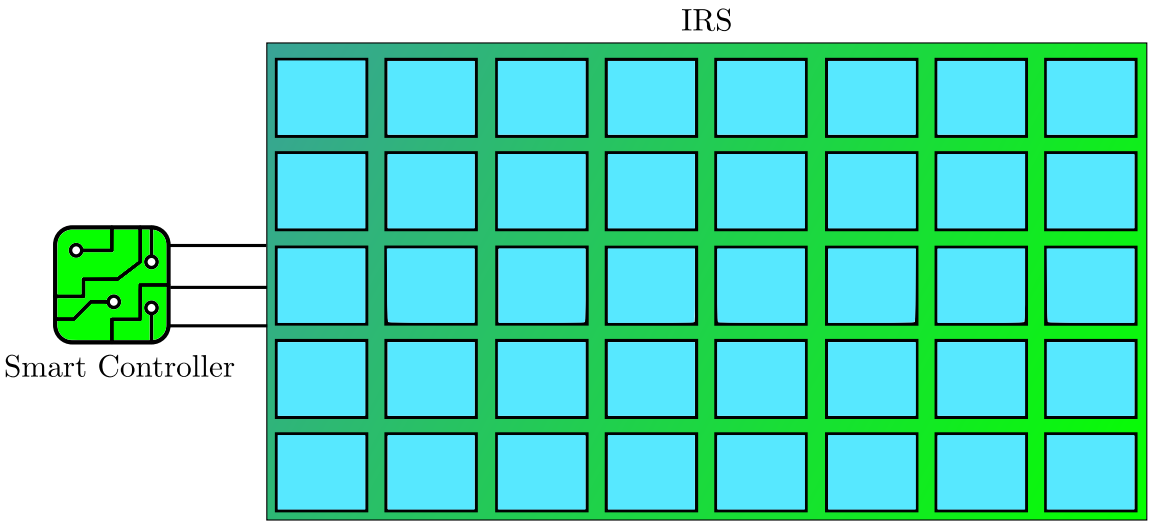

Source: Produced by the author.

(YOU; ZHANG, 2021) addresses the question of which is the better implementation scheme by analysing scenarios of downlink/uplink and optimizing the IRS placement for rate maximization for each. By doing that, it reaches the conclusion that the passive IRS outperforms its active counterpart in scenarios with a sufficiently large number of elements per IRS or when the power amplification from the active IRS is too small.

Architecture and Hardware

One of the main difficulties in physically implementing the IRS is the requirement of a highly configurable metasurface[2] (CUI et al., 2014). Usually, these metasurfaces have parameters that are unchangeable after its manufacture. The set of geometry shape, size and orientation produces a specific metasurface for a specific scenario. Howsoever, in wireless communications we have time-varying channels due to large-scale and small-scale fading effects, consequentially a real-time configurable metasurface to have a proper IRS that can optimize its reflection is desirable.

The IRS is typically composed of three layers and a smart controller (WU; ZHANG, et al., 2021). In Figure 2.4 we shown the basic architecture following the example of (WU; ZHANG, et al., 2021). The first layer of an IRS is where the incident signal will be directly manipulated by the dielectric substrate. In the second layer, a copper plate is placed to maximize the energy efficiency by reducing energy leakage. The third layer is where the circuit board will be placed to excite the first layer as necessary. Finally, the smart controller will be responsible for controlling the link between the IRS, the Transmitter (TX) and Receiver (RX) while adjusting the reflection to its optimal design.

Figure 2.4 IRS's basic architecture.

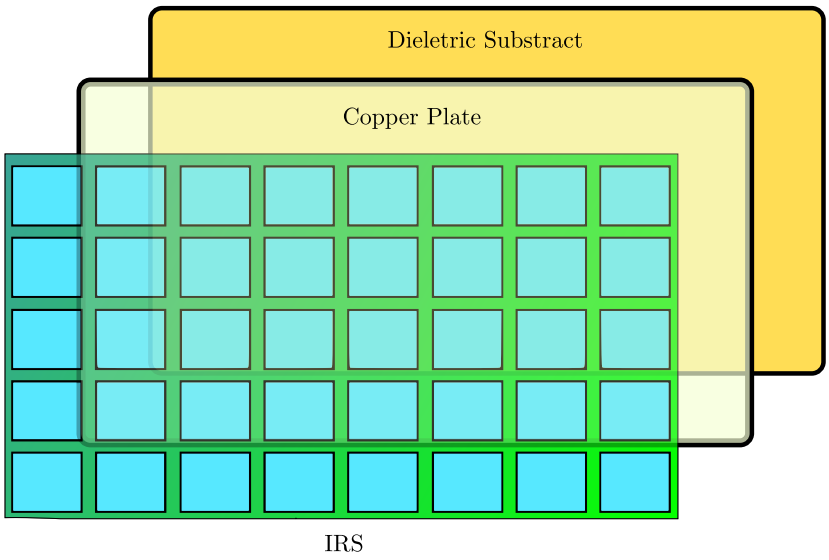

Source: Produced by the author.

At the moment, the design of the third layer is one of the open problems when it comes to the IRS practical design. (WU; ZHANG, 2019) propose an approach to design the third layer by using Positive-Intrinsic-Negative (PIN) diodes that can be in a "ON" or "OFF" state. There are also proposals to use reflector antennas with liquid-crystal-loaded[3]

[2]Metasurfaces are a state-of-art optical device composed of periodic subwavelength metal and dielectric structures(BADLOE et al., 2017). They work by resonant coupling of electric and/or magnetic components of incident lights to produce an effective response that cannot be found in nature (BADLOE et al., 2017).

[3]The liquid-crystal-loaded units makes use of dielectric anisotropy properties and by varying the direct current voltage in the layer the phase-shift can be configurable along the metasurface as desired (FOO, 2017).

metasurfaces (FOO, 2017) or graphene[4] because its conductivity (MA et al., 2020).

Practical Constraints

In practice, usually it is necessary to implement discrete phase-shift and amplitude so we can further reduce the implementation cost and its complexity. To achieve a balance in the trade-off between hardware cost and design complexity we should choose the quantization of the phase-shift or the amplitude (WU; ZHANG, et al., 2021). The real amplitude is far from being a binary value. However, in order to analyze only the impact of the phase-shift quantization, we consider that $\beta_n = 1 \forall n \in N$ for now.

Figure 2.5 Impact of quantization in the IRS's performance.

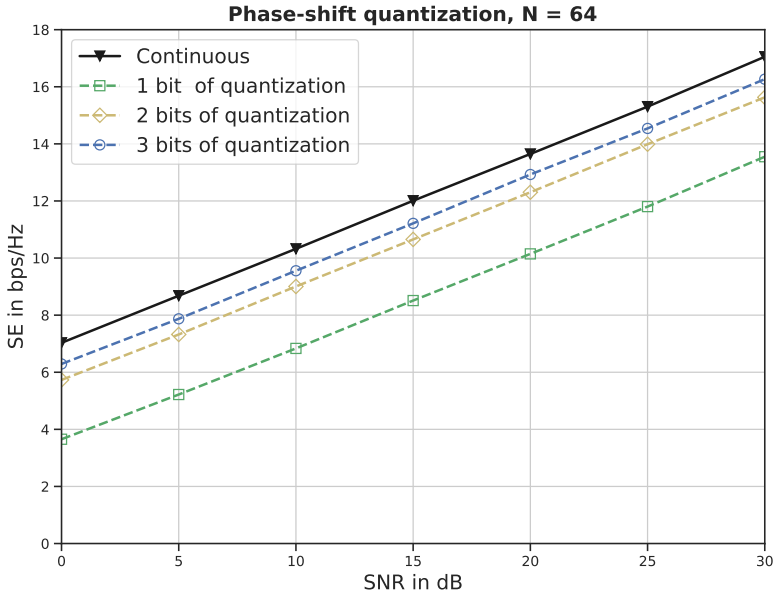

Source: Produced by the author.

The number of phase-shit levels are obtained by simply using $K = 2^{\text{Bits}}$, this way we can design a dictionary of phase-shift values. By using Equation (2.24) we can compute the passive beamforming of a IRS-aided SISO system and its Spectral Efficiency (SE). In Figure 2.5 we can see the impact of the quantization in an IRS with $N = 64$ configurable element. In practice, one PIN diode can represent two levels of quantization since it can be in an "ON" or "OFF" state (WU; ZHANG, et al., 2021). In order to increase the size of the dictionary of phase-shifts, more PIN diodes should be placed, which will result in a higher implementation cost.

Besides, there is still the problem of the non-linear coupling between the amplitude reflection and the phase-shift. It is natural to think that a greater performance can be achieved if we can independently control the amplitude and the phase-shift in a way to obtain a more flexible IRS. (ABEYWICKRAMA et al., 2020) explain how challenging it is to effectively decoupling the design of these two parameters and how this problem leads

[4]Two-dimensional carbon material that has exceptionally high crystal and electronic quality (GEIM; NOVOSELOV, 2010).

to an interesting trade-off between hardware cost and IRS's reflection performance while also proposing an interesting model for the IRS practical implementation using resonant circuits. In addition, a practical reflection model is propose to address this problem as

$$\beta_n(\theta_n) = (1 - \beta_{\min})\Big(\frac{\sin(\theta_n - \phi) + 1}{2}\Big)^{\alpha} + \beta_{\min}, \tag{2.10}$$

where $\beta_{\min} \geq 0$, $\phi \geq 0$, and $\alpha \geq 0$ are constants related to the specific circuit implementation and are fixed once fabricated. By using this equation we can establish the practical relation between the reflection amplitude and the phase-shift.

Figure 2.6 Practical relation between the amplitude and the phase-shift.

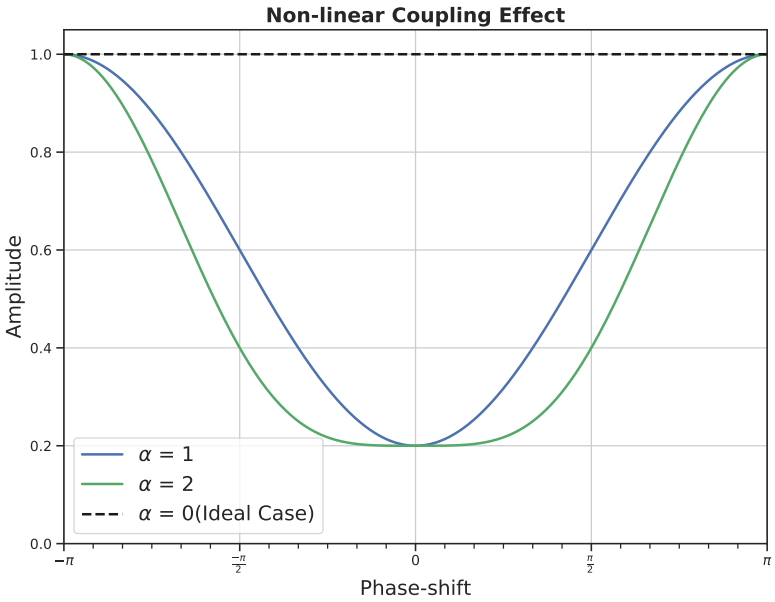

Source: Produced by the author.

As we can observe, the amplitude and the phase-shift of the nth-element are related with each other through a non-linear relation. Thus, the values of amplitude that can effectively interfere with a incident signal at the IRS is a non-integer between 0.2 and 1. For instance, if we want that the IRS changes the phase of a incident signal by an angle close to zero[5] the IRS will reflect it with an attenuation that will greatly reduce its performance. In (ABEYWICKRAMA et al., 2020) this phenomenon is explained by the energy dissipation at the dielectric and other imperfections from the IRS's circuit.

With that in mind it is important to clarify that in this work we will consider the amplitude and the phase-shift as continuous variables. Furthermore, in this work we will not consider the coupling effect between the phase-shift and the amplitude response. Nonetheless, these two extensions remains as a possibility to be analyzed in future works.

[5]In this case the nth element of the IRS is being set to a "OFF" state. So in practice, even if a particular element is set to not reflect the incident signal it still can contribute to the channel interference.

2.3.2 Deployment Strategy

If we have a limited number of reflective elements, N, then how should we proceed to maximize our transmission rate? In (WU; ZHANG, et al., 2021), two optimal IRS deployment strategies are discussed.

- Centralized: A single IRS holding all the available reflective elements.
- Decentralized: Multiple IRSs holding the same fraction of the total number of available reflective elements.

Usually, the centralized deployment is more favorable than its decentralized counterpart since it can achieve higher transmission rates considering the scenario with multiple users (WU; ZHANG, et al., 2021). However, a detailed research of this problem is something out of scope of this work.

2.4 IRS-Aided SISO Systems

In this section we discuss the scenario of an IRS-aided SISO systems and its channel and signal models. The concept of passive beamforming and power scaling will be briefly discussed at the end of this section.

2.4.1 Received Signal Model

Figure 2.7 Single IRS-aided SISO system.

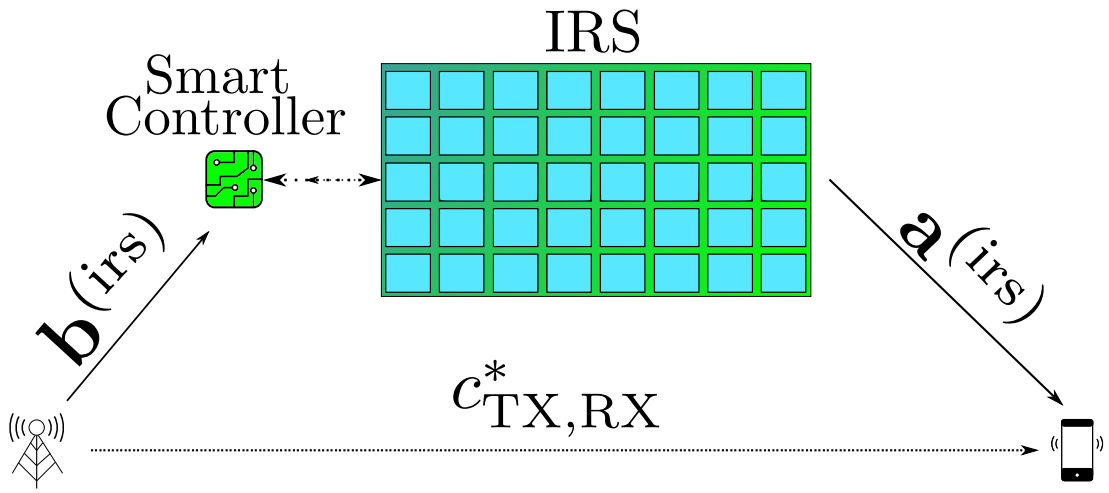

Source: Produced by the author.

We can obtain the received signal model for an IRS-aided SISO system considering a scenario where a single IRS with N elements is placed between the TX and the RX as in Figure 2.7. $c^*_{TX,RX}$ is the direct channel between TX and RX. Furthermore, the TX and the RX will be equipped with a single antenna. As explained in great details in (WU; ZHANG, et al., 2021), considering that the carrier frequency (f_c) and the system bandwidth (B) follow the relation $B \lll f_c$, the baseband signal model for the nth element is given by

$$y_n = \left(\beta_n e^{j\theta_n} a_n^* b_n + c^*_{TX,RX}\right) x, \tag{2.11}$$

where b_n is the channel between the TX and the nth element, $\beta_n e^{j\theta_n}$ is the IRS phase-shift and amplitude response, a_n^* is the channel between the nth element and the RX, $c^*_{TX,RX}$ is the direct link between TX and RX and x is the pilot signal. Finally, the baseband received signal model that account for all the N IRS elements can be expressed by

$$y = \left(\sum_{n=1}^{N} \beta_n e^{j\theta_n} a_n^* b_n + c^*_{TX,RX}\right) x, \tag{2.12}$$

where x will be an information signal and β_n represents the individual state of a particular IRS's element. It is important to reaffirm that β_n will have only binary values, since the (semi-) passive IRS can not amplify incident signals. Furthermore, if we define

$$\mathbf{a}^{(\text{irs})\text{H}} = [a_1^*, a_2^*, \cdots, a_N^*], \tag{2.13}$$

$$\mathbf{b}^{(\text{irs})} = [b_1, b_2, \cdots, b_N], \tag{2.14}$$

$$\mathbf{s} = \text{diag}(\beta_1 e^{j\theta_1}, \ldots, \beta_N e^{j\theta_N})^{\text{T}}, \tag{2.15}$$

then we can rewrite Equation (2.12) as

$$y = \left(\mathbf{a}^{(\text{irs})\text{H}} \text{diag}\left(\mathbf{s}\right) \mathbf{b}^{(\text{irs})} + c^*_{TX,RX}\right) x. \tag{2.16}$$

From Equation (2.16), as already highlighted by (WU; ZHANG, et al., 2021), we can notice that the IRS is essentially performing a linear mapping from the incident signal to a reflected signal. The diagonal matrix, i.e., $\text{diag}\left(\mathbf{s}\right)$, is explained by the fact the each reflection is considered to be independent, thus discarding any interference from signal coupling or joint processing. It is also worth noting that the channel coefficients in $\mathbf{a}^{(\text{irs})\text{H}}$ and $\mathbf{b}^{(\text{irs})}$ usually depend on distance-related path loss (WU; ZHANG, et al., 2021).

2.4.2 Passive Beamforming

In this section, the optimum IRS phase-shift design is derived, based on the received signal mode from previously section. Considering the received signal model in Equation (2.16), by taking into account the transmitted power P_t and the additive noise term v, rewriting it as in (WU; ZHANG, et al., 2021)

$$y = (\mathbf{a}^{(\text{irs})\text{H}} \text{diag}\left(\mathbf{s}\right) \mathbf{b}^{(\text{irs})} + c^*_{TX,RX})\sqrt{P_t} x + v, \tag{2.17}$$

where x is the information signal, P_t is the transmitted power, and v is modeled as an Additive White Gaussian Noise (AWGN)[6] with zero mean and variance σ^2. The received SNR is given by

$$\gamma = \frac{||(\mathbf{a}^{(\text{irs})\text{H}} \text{diag}\left(\mathbf{s}\right) \mathbf{b}^{(\text{irs})} + c^*_{TX,RX})\sqrt{P_t} x||^2}{\sigma^2}, \tag{2.18}$$

$$= \frac{||\mathbf{a}^{(\text{irs})\text{H}} \text{diag}\left(\mathbf{s}\right) \mathbf{b}^{(\text{irs})} + c^*_{TX,RX}||^2 P_t x^2}{\sigma^2}, \tag{2.19}$$

$$= \frac{||\sum_{n=1}^{N} \beta_n e^{j\theta_n} a_n^* b_n + c^*_{TX,RX}||^2 P_t x^2}{\sigma^2}. \tag{2.20}$$

Our objective is to maximize the SNR at the receiver by optimizing the passive beamforming at the IRS. By neglecting the constant terms, transmitted power P_t and pilot signal x, we formulate an optimization problem as

[6] This is a well-known noise model where its components are directly add to the information signal with an uniform power distribution within all the transmission frequencies from that communication system. Nonetheless, the Gaussian terminology refers that the samples of this noise model are picked from a normal distribution with mean μ and variance σ^2.

$$\max_{\theta_n,\beta} \quad \Big|\Big| \sum_{n=1}^{N} \beta_n e^{j\theta_n} a_n^* b_n + c_{TX,RX}^* \Big|\Big|^2 \tag{2.21}$$

$$\text{s.t.} \quad 0 \leq \theta_n \leq 2\pi, \forall n \in \{1, \cdots, N\} \tag{2.22}$$

$$0 \leq \beta_n \leq 1, \forall n \in \{1, \cdots, N\}. \tag{2.23}$$

The maximum possible value for the amplitude response, without power amplification, $\beta_n = 1 \forall n \in N$, meaning that no power dissipation or attenuation is considered to occur at the IRS. By replacing this condition in Equation (2.21) all that is left for us to solve this optimization problem is to obtain the expression for the optimal phase, θ_n. In (WU; ZHANG, et al., 2021) the solution for this remaining optimization is the expression

$$\begin{aligned} \theta_n &= \zeta - (\phi_n + \psi_n), \forall n \in \{1, \cdots, N\}, \\ e^{j\theta_n} &= e^{j(\zeta - (\phi_n + \psi_n))}, \forall n \in \{1, \cdots, N\}, \end{aligned} \tag{2.24}$$

where ϕ_n, ψ_n, and ζ are the phases of a_n^*, b_n, and $c_{TX,RX}^*$ respectively. This solution could be viewed as an alignment between the signals, incident and reflected, and the IRS's elements. If we consider that the direct channel between TX and RX is negligible then we have $c_{TX,RX}^* = 0$ and consequently $\zeta = 0$. Replacing (2.24) into Equation (2.20) we obtain

$$\begin{aligned} \gamma &= \Big|\Big| \sum_{n=1}^{N} e^{j\theta_n} a_n^* b_n \Big|\Big|^2, \\ &= \Big|\Big| \sum_{n=1}^{N} e^{-j(\phi_n + \psi_n)} ||a_n^*|| e^{j\psi_n} ||b_n|| e^{j\phi_n} \Big|\Big|^2, \\ &= \Big|\Big| \sum_{n=1}^{N} ||a_n^*|| ||b_n|| \Big|\Big|^2, \\ &= N^2 ||\mathbf{a}^{\text{irs}}|| ||\mathbf{b}^{\text{irs}}||. \end{aligned} \tag{2.25}$$

Equation (2.25) displays one of the most interesting aspects of the IRS that is the SNR scaling with N at the intended receiver. This equation suggests that the SNR at the receiver increases quadratically with N, but of course this is not a magical solution to achieve a better performance considering other orthodoxes methods like relaying as already discussed in Section 2.3.1. Nonetheless, it is important to note that the IRS optimization design depends only of the cascaded channels that pass through the IRS (WU; ZHANG, et al., 2021). Therefore, we do not need to know the individual channels to properly optimize the IRS.

2.5 IRS-Aided MIMO Systems

In this section we will focus our attention to concepts of MIMO system and the notion capacity, multiplexing and active beamforming. By the end we offer a basic insight of how we should approach a scenario of IRS-aided MIMO systems considering the contributions of (ARAÚJO et al., 2021) and (HE; YUAN, 2019).

2.5.1 MIMO Basics

Figure 2.8 MIMO system with L scatterers

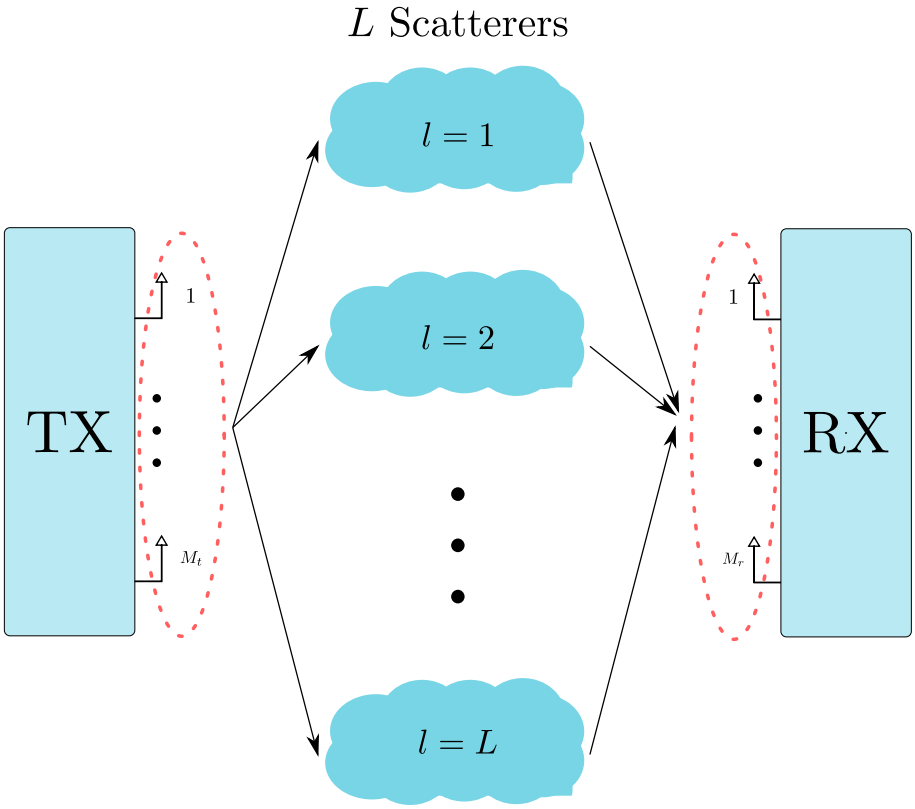

Source: Produced by the author.

As properly explained in (CAVALCANTI et al., 2018), MIMO systems are one the main technologies that, by taking advantage of a specular multipath environment, effectively increasing data rates and reliability in modern wireless communications systems. Figure 2.8 represents a MIMO system where TX and RX are equipped with an Uniform Linear Array (ULA)[7] of M_t and M_r antennas, respectively. In this scenario, we have a specular multipath propagation environment with L natural scatterers that will interfere with the signal propagation. According to (CAVALCANTI et al., 2018) and (GOLDSMITH, 2005) the matrix relation for the received signal at RX will be

[7](VAN TREES, 2001) a vector where its elements are uniformly placed in a way that any pair of consecutive elements will be always at the same distance.

$$\mathbf{y} = \mathbf{H}\mathbf{x} + \mathbf{v} \in \mathbb{C}^{M_r \times 1}, \tag{2.26}$$

where $\mathbf{x} \in \mathbb{C}^{M_t \times 1}$ is the transmitted signal, $\mathbf{v} \sim \mathcal{CN}(0, \sigma^2_{\text{noise}})$ is the AWGN vector at RX, and $\mathbf{H} \in \mathbb{C}^{M_r \times M_t}$ is the channel coefficient matrix. In this scenario, the channel matrix $\mathbf{H}$ can be defined by

$$\mathbf{H} = \sum_{l=1}^{L} \gamma_l \, \mathbf{a}_l^{(\text{rx})} \mathbf{b}_l^{(\text{tx})\text{T}} \in \mathbb{C}^{M_r \times M_t}, \tag{2.27}$$

where γ_l contains the path loss and fast-fading components associated with the scatter at the lth path, $\mathbf{a}_l^{(\text{rx})}$, and $\mathbf{b}_l^{(\text{tx})\text{T}}$ are the steering vectors of TX-lth path and lth path-RX, respectively. In (VAN TREES, 2001), the steering vectors are given by

$$\mathbf{a}_l^{(\text{rx})} = [1, ..., e^{-j\pi(M_r-1)\cos(\alpha_l)}]^{\text{T}} \in \mathbb{C}^{M_r \times 1}, \tag{2.28}$$
$$\mathbf{b}_l^{(\text{tx})} = [1, ..., e^{-j\pi(M_r-1)\cos(\beta_l)}]^{\text{T}} \in \mathbb{C}^{M_t \times 1}, \tag{2.29}$$

where α_l and β_l denote the Angle of Arrival (AoA) and Angle of Departure (AoD) of the l-th path, respectively.

Capacity

The capacity of a communication system, also known as Shannon Capacity, can be used to indicate the achievable data rate of the system. This means the amount of information that the system can properly transmit and receive within an acceptable level of reliability. According to (GOLDSMITH, 2005), the capacity of wireless channels is

$$\text{C(bps)} = \text{B} \log_2(1 + \gamma), \tag{2.30}$$

where γ represents the SNR of the channel. If we divide the expression above by the bandwidth of the system, B, then we obtain the Spectral Efficiency (SE) of the channel as

$$\text{SE(bps/Hz)} = \log_2(1 + \gamma). \tag{2.31}$$

Besides the SNR there is also the the Signal-to-Interference-plus-Noise Ratio (SINR) that we can use to account the contribution of interference signals and the background noise to the wireless channels. This way we could see the impact of special phenomena intrinsic to wireless communication systems (large-scale fading, small-scale fading, etc). One of the ways to deal with these phenomena is by using multiplexing techniques that will be discuss in the next section.

Multiplexing and Active Beamforming

As explained in (GOLDSMITH, 2005), by having multiple antennas at the transmitter and at the receiver we can exploit this to obtain parallel independent channels that are used to increase the capacity of the system. Supposing that Rank($\mathbf{H}$)= $R_{\mathbf{H}}$, it is possible to decompose the channel in R parallel independent channels. By transmitting independent data streams into these parallel channels we increase the transmission data rate. This is called spatial multiplexing and if we consider the MIMO system from Figure 2.8 it is possible to write the channel matrix with the Single Value Decomposition (SVD) as

$$\mathbf{H} = \mathbf{U}\mathbf{\Sigma}\mathbf{V}^{\mathrm{H}}, \tag{2.32}$$

then we can formally define the channel rank as the number $R_{\mathbf{H}}$ of singular values from $\mathbf{\Sigma}$ that are different from zero. Since the rank indicates the number of linear independent columns/rows of a given matrix we can write the relation

$$R_{\mathbf{H}} \geq \min(M_t, M_r). \tag{2.33}$$

The rank indicates the quantity of independent data streams that we can transmit and recover at the end of transmission and by having $R_{\mathbf{H}} \geq \min(M_t, M_r)$ we can classify our scenario as a rich scattering environment. To design a ideal pair of precoder and combiner we need to assume that the both transmitter and receiver have a perfect knowledge from the CSI. Following (PAULRAJ et al., 2003), and (GOLDSMITH, 2005) instructions we can design the precoder $\mathbf{W}$ and the combiner $\mathbf{Q}$ by the two following relations, if we have a perfect knowledge of the CSI at Equation (2.32)

$$\mathbf{Q} = \mathbf{V}^{\mathrm{H}} \in \mathbb{C}^{M_t \times R_{\mathbf{H}}}, \tag{2.34}$$
$$\mathbf{W} = \mathbf{U} \in \mathbb{C}^{M_r \times R_{\mathbf{H}}}, \tag{2.35}$$

this way the transmitted signal $\mathbf{x}$ and the received signal $\mathbf{y}$ will be redefined as

$$\overline{\mathbf{x}} = \mathbf{Q}^{\mathrm{H}}\mathbf{x} = \mathbf{V}\mathbf{x}, \tag{2.36}$$
$$\overline{\mathbf{y}} = \mathbf{W}^{\mathrm{H}}\mathbf{y} = \mathbf{U}^{\mathrm{H}}\mathbf{y}, \tag{2.37}$$

replacing $\mathbf{x}$, and $\mathbf{y}$ by their beamformings at Equation (2.26) and replacing $\mathbf{H}$ by (2.32) we obtain a new relation for the MIMO system

$$\begin{aligned}
\overline{\mathbf{y}} &= \mathbf{U}^{\mathrm{H}}(\mathbf{H}\mathbf{V}\overline{\mathbf{x}} + \mathbf{v}), \\
&= \mathbf{U}^{\mathrm{H}}\mathbf{H}\mathbf{V}\overline{\mathbf{x}} + \mathbf{W}^{\mathrm{H}}\mathbf{v}, \\
&= \mathbf{U}^{\mathrm{H}}\mathbf{U}\mathbf{\Sigma}\mathbf{V}^{\mathrm{H}}\mathbf{V}\overline{\mathbf{x}} + \mathbf{U}^{\mathrm{H}}\mathbf{v}, \\
&= \mathbf{\Sigma}\overline{\mathbf{x}} + \overline{\mathbf{v}},
\end{aligned} \tag{2.38}$$

where $\mathbf{U}^{\mathrm{H}}\mathbf{U} = \mathbf{I}_{M_r}$ and $\mathbf{V}^{\mathrm{H}}\mathbf{V} = \mathbf{I}_{M_t}$ since by definition the matrices of eigenvectors from a SVD are unitary. With Equation (2.38) we can see that our channel now is parallelized, meaning that a single symbol from $\mathbf{x}$ is being transmitted over a single parallel channel from the diagonal matrix Σ. Finally we can write $\overline{\mathbf{v}} = \mathbf{U}^{\mathrm{H}}\mathbf{v}$, but the unitary matrix, $\mathbf{U}^{\mathrm{H}}$, will not affect the statistical properties of the noise vector (GOLDSMITH, 2005).

Multiplexing Gain

As mentioned in (GOLDSMITH, 2005), by considering the contribution of each independent parallel channel we can obtain the following relation for the capacity of a static MIMO system

$$\mathrm{C(bits/second)} = \mathbb{E}[\mathbf{y}\mathbf{y}^{\mathrm{H}}]. \tag{2.39}$$

If we consider the equivalent MIMO channel, precoder and combiner included, as $\mathbf{H}_{\mathrm{eq}} = \mathbf{W}^{\mathrm{H}}\mathbf{H}\mathbf{Q}$ and use Equation (2.26) at Equation (2.39) we can write the capacity of a MIMO system as

$$\mathrm{C(bps)} = B\ \log_2\Big[\det\Big(\mathbf{I}_{M_r} + \frac{\mathbf{H}\mathbf{R}_{xx}\mathbf{H}^{\mathrm{H}}}{\sigma^2_{\mathrm{noise}}}\Big)\Big], \tag{2.40}$$

$$\mathrm{SE(bps/Hz)} = \ \log_2\Big[\det\Big(\mathbf{I}_{M_r} + \frac{\mathbf{H}\mathbf{R}_{xx}\mathbf{H}^{\mathrm{H}}}{\sigma^2_{\mathrm{noise}}}\Big)\Big], \tag{2.41}$$

where $\mathrm{trace}\left(\mathbf{Q}\mathbf{R}_{xx}\mathbf{Q}^{\mathrm{H}}\right) = \mathbf{I}_{M_t}$. Maybe it is not clear in the matrix format, but Equation (2.40) is basically collecting the contributions of each pair $M_r - M_t$ of antennas and adding it to the total value of capacity.

2.5.2 IRS-Aided MIMO Systems

The work of (ARAÚJO et al., 2021) consider a MIMO system assisted by a single IRS and a supervised(pilot-assisted) method to obtain the CSI is proposed. In this scenario, the TX (Base Station) and the RX (User Terminal) are equipped with arrays of M and L antennas, respectively, and the IRS is composed of N configurable elements. The signal model for this scenario is given as (HE; YUAN, 2019)

$$\mathbf{y}[t] = \mathbf{G}(\mathbf{s}[t] \odot \mathbf{H}\mathbf{x}[t]) + \mathbf{b}[t], 1 \leq t \leq T \tag{2.42}$$

where $\mathbf{x}[t] \in \mathbb{C}^{M\times 1}$ is the vector of transmitted pilot signals at t, $\mathbf{s}[t] \in \mathbb{C}^{N\times 1}$ is the vector of IRS's phase-shift that will explained in details in the next chapter and $\mathbf{b}[t]$ is the AWGN component. Finally, $\mathbf{H} \in \mathbb{C}^{N\times M}$ and $\mathbf{G} \in \mathbb{C}^{L\times N}$ represent the MIMO channels from TX-IRS and IRS-RX, respectively. The channel goes through a training process composed of K blocks where each one is divided in T time-slots. From Equation (2.42) and with some algebraic manipulations is possible to write a tensor approach for this scenario as

$$\overline{\mathbf{y}} = \begin{bmatrix} \mathbf{y}[1] \\ \vdots \\ \mathbf{y}[T] \end{bmatrix}, \tag{2.43}$$

$$= [\mathbf{S} \otimes (\mathbf{X} \otimes \mathbf{I}_L)]\text{vec}(\mathbf{H}^{\text{T}} \diamond \mathbf{G}) + \mathbf{b} \in \mathbb{C}^{LTK}, \tag{2.44}$$

where $\mathbf{S} = [\mathbf{s}[1], \cdots, \mathbf{s}[K]]^{\text{T}} \in \mathbb{C}^{K \times N}$, $\mathbf{X} = [\mathbf{x}[1], \cdots, \mathbf{x}[T]]^{\text{T}} \in \mathbb{C}^{T \times M}$. The process to obtain the equation above is detailed in (ARAÚJO et al., 2021) and show us the basic insight of how we should approach a scenario of an IRS-aided MIMO system, although it goes into the direction of tensor algebra. Then, two methods to obtain the Channel State Information (CSI) are proposed and by decoupling the estimates of the MIMO channel matrices it is possible too enhance the algorithm performance in comparison to methods that estimate only the cascaded of the channels that pass through the IRS.

3 System Model

This chapter in divided in three main sections. In Section 3.1 we present the proposed scenario of Multi-IRS MIMO. In Section 3.2, we discuss two approaches for channel estimation and propose design recommendations. In Section 3.3, we discuss the proposed algorithm the joint beamforming and channel estimation.

3.1 Multi-IRS MIMO

Figure 3.1 MIMO communication system assisted by multiple IRSs. The signal from the transmitter to the receiver propagates *via* P dominant scatterers. An IRS panel is placed at the exact location of each scatterer.

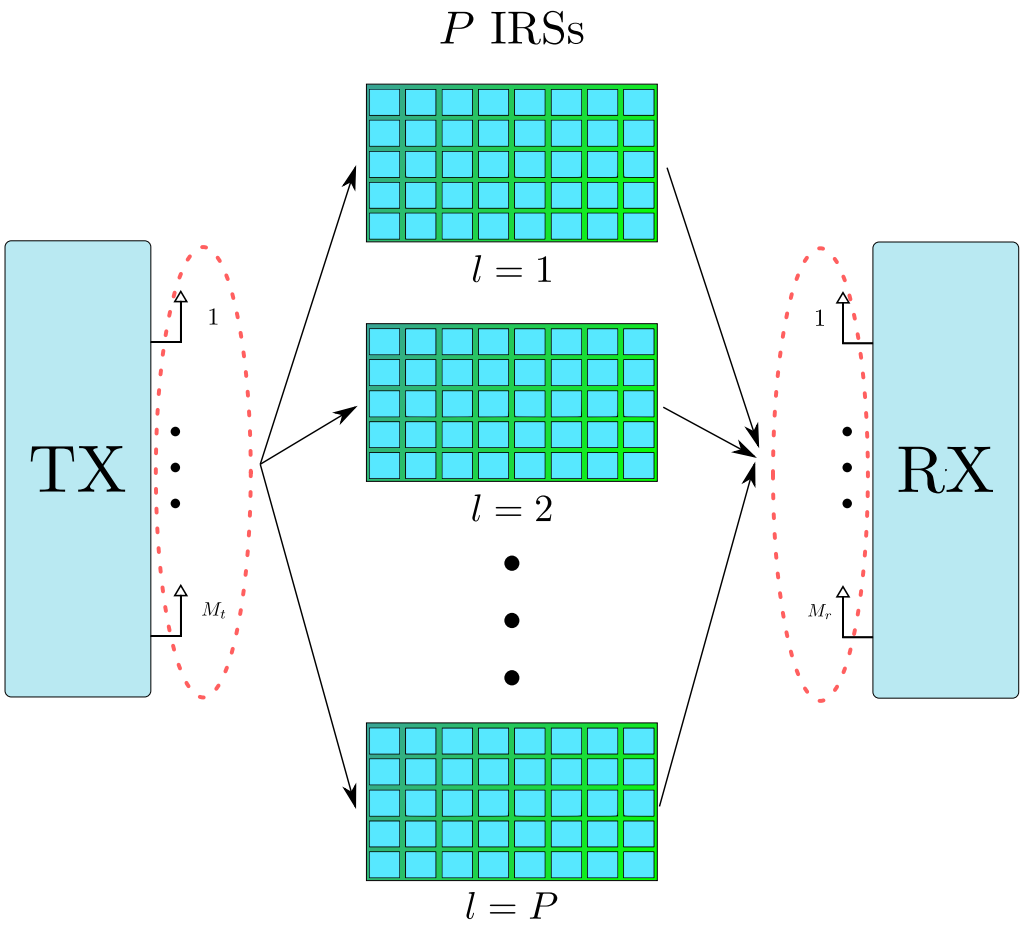

Source: Produced by the author.

As briefly explained in Section 2.5.1, let us consider a MIMO system where the TX and RX are equipped with ULA, having M_t and M_r antennas, respectively. We assume a specular multipath propagation environment with P dominant scatterers. The received signal follows the previously explained input-output relation:

$$\mathbf{y} = \mathbf{H}\mathbf{x} + \mathbf{v} \in \mathbb{C}^{M_r \times 1}, \tag{3.1}$$

where $\mathbf{x} \in \mathbb{C}^{M_t \times 1}$ is the transmitted signal, $\mathbf{v} \in \mathbb{C}^{M_r \times 1}$ is the AWGN at the RX, while the channel matrix $\mathbf{H} \in \mathbb{C}^{M_r \times M_t}$ can be modeled as

$$\mathbf{H} = \sum_{p=1}^{P} \gamma_p \mathbf{a}_p^{(\mathrm{rx})} \mathbf{b}_p^{(\mathrm{tx})T} \in \mathbb{C}^{M_r \times M_t}, \tag{3.2}$$

where γ_p contains the path loss and the fast-fading components associated with the pth scatterers, $\mathbf{a}_p^{(\mathrm{rx})}$ and $\mathbf{b}_p^{(\mathrm{tx})\mathrm{T}}$ are the pth steering vectors, which are defined once again as in (VAN TREES, 2001)

$$\mathbf{a}_p^{(\mathrm{rx})} = [1, ..., e^{-j\pi(M_r-1)\cos(\alpha_p)}]^{\mathrm{T}} \in \mathbb{C}^{M_r \times 1} \tag{3.3}$$
$$\mathbf{b}_p^{(\mathrm{tx})} = [1, ..., e^{-j\pi(M_t-1)\cos(\beta_p)}]^{\mathrm{T}} \in \mathbb{C}^{M_t \times 1}, \tag{3.4}$$

where α_p and β_p denote the AoA and AoD of the p-th path, respectively.

Let us assume that these P scatterers were identified, e.g., via some channel sounding method similar to (SALMI et al., 2008), and that it is possible to place P IRSs at the location of these scatterers, as illustrated in Figure 3.1. Different from the usual IRS-aided MIMO system model considered in the literature (ARAÚJO et al., 2021), (WEI et al., 2021), (ARDAH et al., 2021), (WANG, Z. et al., 2020), where the IRS is placed between the scatterers linking the TX and the RX, in this work we propose to study the effect of having multiple IRSs, each of which placed at the the exact location of the channel scatterers. Considering that the training sequences have a duration of $K \cdot P$ symbol periods as illustrated in Figure 3.2, the received pilot signals collected in the vector $\mathbf{y}_k \in \mathbb{C}^{M_r \times 1}$ for the kth time slot can be written as

$$\mathbf{y}_k = \boldsymbol{\gamma} \mathbf{A} \mathrm{diag}_k\left(\mathbf{S}^{(p)}\right) \mathbf{B} \mathbf{x}_k + \mathbf{v}_k \in \mathbb{C}^{M_r \times 1}, \tag{3.5}$$
$$\mathbf{y}_k = \sum_{p=1}^{P} \gamma_p \mathbf{a}_p^{(\mathrm{rx})} \mathbf{a}_p^{(\mathrm{irs})\mathrm{T}} \mathrm{diag}_k\left(\mathbf{S}^{(p)}\right) \mathbf{b}_p^{(\mathrm{irs})} \mathbf{b}_p^{(\mathrm{tx})\mathrm{T}} \mathbf{x}_k + \mathbf{v}_k \in \mathbb{C}^{M_r \times 1}, \tag{3.6}$$

where $\mathbf{x}_k \in \mathbb{C}^{M_r \times 1}$ is the pilot symbol transmitted at the kth time slot, $\mathbf{a}_p^{(\mathrm{irs})} \in \mathbb{C}^{N \times 1}$ and $\mathbf{b}_p^{(\mathrm{irs})} \in \mathbb{C}^{N \times 1}$ are the IRS array steering vectors associated with the p-th arrival and departure angles, respectively. Since the IRS is a 2D panel, each AoA and AoD has azimuth and elevation responses. Based on the formulation of a Uniform Rectangular Array (URA)[1] (VAN TREES, 2001), we can write the arrival steering vector of the IRS as

$$\mathbf{b}_p^{(\mathrm{irs})} = \mathbf{b}_p^{v(\mathrm{irs})} \otimes \mathbf{b}_p^{h(\mathrm{irs})} \in \mathbb{C}^{N_h N_v \times 1},$$

with $N_h N_v = N$, and $\mathbf{b}_p^{h(\mathrm{irs})}$ and $\mathbf{b}_p^{v(\mathrm{irs})}$ being the azimuth and elevation steering vectors, respectively. The nth element of $\mathbf{b}_p^{(\mathrm{irs})}$ is given by

[1] (VAN TREES, 2001) similar to the definition of an ULA but this time we have a 2D array in which its elements are uniformly spaced.

$$\left[\mathbf{b}_p^{(\text{irs})}\right]_{n_h+(n_v-1)N_h} = e^{j\pi\left((n_h-1)\cos\phi_p^b\sin\psi_p^b+(n_v-1)\cos\phi_p^b\right)},$$

with $n_h = \{1,\ldots,N_h\}$, $n_v = \{1,\ldots,N_v\}$, and $n = n_h + (n_v-1)N_h$, where ϕ_p^b and ψ_p^b are azimuth and elevation AoAs, respectively. Similarly, the departure steering vector of the IRS also has the same Kronecker structure, i.e.,

$$\mathbf{a}_p^{(\text{irs})} = \mathbf{a}_p^{v(\text{irs})} \otimes \mathbf{a}_p^{h(\text{irs})} \in \mathbb{C}^{N_h N_v \times 1},$$

where the nth element of $\mathbf{a}_p^{(\text{irs})}$ is given by

$$\left[\mathbf{a}_p^{(\text{irs})}\right]_{n_h+(n_v-1)N_h} = e^{j\pi\left((n_h-1)\cos\phi_p^a\sin\psi_p^a+(n_v-1)\cos\phi_p^a\right)},$$

with ϕ_p^a and ψ_p^a being the azimuth and elevation AoDs, respectively.

In Equation (3.6), $\mathbf{S}^{(p)} \in \mathbb{C}^{N\times K}$ is the matrix that contains the IRS phase-shifts associated with the p-th IRS, which are collected in the following matrix

$$\mathbf{S}^{(p)} = \begin{bmatrix} \beta_{1,1}^{(p)} e^{j\theta_{1,1}^{(p)}} & \beta_{1,2}^{(p)} e^{j\theta_{1,2}^{(p)}} & \cdots & \beta_{1,K}^{(p)} e^{j\theta_{1,K}^{(p)}} \\ \beta_{2,1}^{(p)} e^{j\theta_{2,1}^{(p)}} & \beta_{2,2}^{(p)} e^{j\theta_{2,2}^{(p)}} & \cdots & \beta_{2,K}^{(p)} e^{j\theta_{2,K}^{(p)}} \\ \vdots & \vdots & \ddots & \vdots \\ \beta_{N,1}^{(p)} e^{j\theta_{N,1}^{(p)}} & \beta_{N,2}^{(p)} e^{j\theta_{N,2}^{(p)}} & \cdots & \beta_{N,K}^{(p)} e^{j\theta_{N,K}^{(p)}} \end{bmatrix} \in \mathbb{C}^{N\times K}, \tag{3.7}$$

where $\beta_{n,k} = \{0,1\}$ and $\theta_{n,k}$ are the reflection coefficient and the designed phase-shift for the nth IRS element, respectively for the kth time slot. Meanwhile, $\text{diag}_k\left(\mathbf{S}^{(p)}\right)$ is the diagonal matrix created from the IRS phase-shift k-th column vector

$$\text{diag}_k\left(\mathbf{S}^{(p)}\right) = \begin{bmatrix} \beta_{1,k}^{(p)} e^{j\theta_{1,k}^{(p)}} & 0 & \cdots & 0 \\ 0 & \beta_{2,k}^{(p)} e^{j\theta_{2,k}^{(p)}} & \cdots & 0 \\ \vdots & \vdots & \ddots & \vdots \\ 0 & 0 & \cdots & \beta_{N,k}^{(p)} e^{j\theta_{N,k}^{(p)}} \end{bmatrix} \in \mathbb{C}^{N\times N}. \tag{3.8}$$

3.2 Channel Estimation Methods

Figure 3.2 Time-frame of channel estimation and IRS optimization.

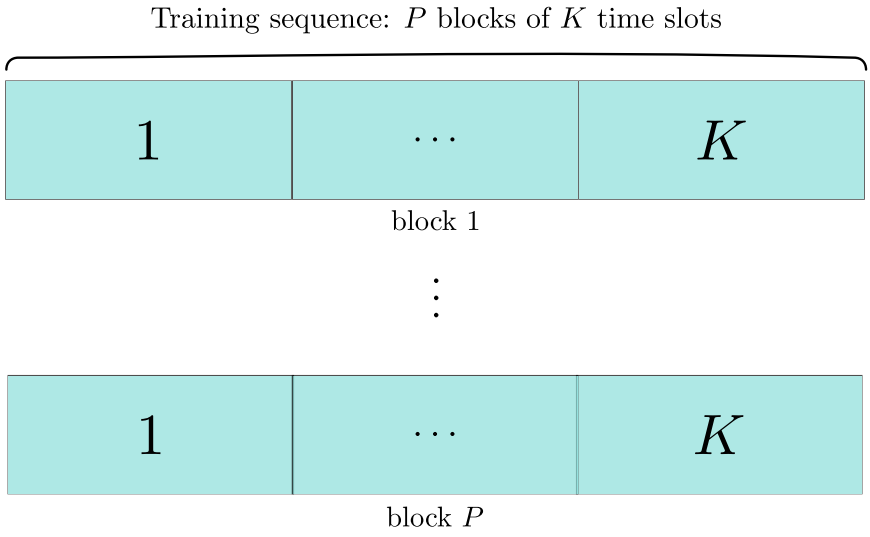

Source: Produced by the author.

In this section we consider two main approaches to the channel estimation problem in the context of IRS. In the first, we consider that the IRS is capable of setting the reflection amplitude element $\beta_{n,k} = 0$. In other words, the IRS is capable of absorb the incoming signal and consequentially, the not intend reflections can be neglected. While in the second approach, we consider that the reflection coefficient cannot be zero, and some part of the incoming signals is always reflected as interference.

3.2.1 IRS Interfering Signals Absorption

For the channel estimation and joint beamforming design, we propose the training sequence protocol shown in Figure 3.2, which is composed with P blocks of size K symbol periods. The main idea is to use these P blocks to reorganize the MIMO problem into P SISO problems. First, let us rewrite Equation (3.6) as

$$\begin{aligned}\mathbf{y}_k = \gamma_1 \mathbf{a}_1^{(\mathrm{rx})} \mathbf{a}_1^{(\mathrm{irs})\mathrm{T}} \mathrm{diag}_k\left(\mathbf{S}^{(1)}\right) \mathbf{b}_1^{(\mathrm{irs})} \mathbf{b}_1^{(\mathrm{tx})\mathrm{T}} \mathbf{x}_k + \mathbf{v}_k^{(1)}, \\ + \underbrace{\sum_{p=2}^{P} \gamma_p \mathbf{a}_p^{(\mathrm{rx})} \mathbf{a}_p^{(\mathrm{irs})\mathrm{T}} \mathrm{diag}_k\left(\mathbf{S}^{(p)}\right) \mathbf{b}_p^{(\mathrm{irs})} \mathbf{b}_p^{(\mathrm{tx})\mathrm{T}} \mathbf{x}_k}_{\text{interference}} \in \mathbb{C}^{M_r \times 1}.\end{aligned} \tag{3.9}$$

Let us assume that, in the first block, the desired signal is the one coming from the first IRS. Thus, the contribution from the remaining IRSs ($p = \{2, \ldots, P\}$) are considered as interference. To eliminate the interference from the received signal $\mathbf{y}_k^{(1)}$, the amplitude reflection $\beta_{n,k}^{(p)}$ from the IRSs, placed at the scatterers $p = \{2, \ldots, P\}$, are set to zero. This

means that they are in absorption mode[2]. Thus, for the first block ($p = 1$), the received pilots can be written as

$$\mathbf{y}_k^{(1)} = \gamma_1 \mathbf{a}_1^{(\mathrm{rx})} \mathbf{a}_1^{(\mathrm{irs})\mathrm{T}} \mathrm{diag}_k\left(\mathbf{S}^{(1)}\right) \mathbf{b}_1^{(\mathrm{irs})} \mathbf{b}_1^{(\mathrm{tx})\mathrm{T}} \mathbf{x}_k + \mathbf{v}_k^{(1)},$$
$$+ \sum_{p=2}^{P} \gamma_p \mathbf{a}_p^{(\mathrm{rx})} \mathbf{a}_p^{(\mathrm{irs})\mathrm{T}} \mathrm{diag}_k\left(\mathbf{S}^{(p)}\right) \mathbf{b}_p^{(\mathrm{irs})} \mathbf{b}_p^{(\mathrm{tx})\mathrm{T}} \mathbf{x}_k \to 0 \in \mathbb{C}^{M_r \times 1}. \tag{3.10}$$

For the training stage, let us assume that all IRSs have the same phase-shift matrix, i.e., $\mathbf{S}^{(1)} = \ldots = \mathbf{S}^{(P)} = \mathbf{S} \in \mathbb{C}^{N \times K}$, and $\mathbf{S}$ is designed as a truncated Discrete Fourier Transform (DFT) matrix[3] of size $N \times K$. Neglecting the noise term, and applying properties (2.5), (2.6) and (2.7) to Equation (3.10), we have

$$\begin{aligned}
\mathbf{y}_k^{(1)} &= \gamma_1 \mathbf{I}_{M_r} \mathbf{a}_1^{(\mathrm{rx})} \mathbf{a}_1^{(\mathrm{irs})\mathrm{T}} \mathrm{diag}_k\left(\mathbf{S}^{(1)}\right) \mathbf{b}_1^{(\mathrm{irs})} \mathbf{b}_1^{(\mathrm{tx})\mathrm{T}} \mathbf{x}_k, \\
&= \gamma_1 \mathrm{vec}\left(\mathbf{I}_{M_r} \mathbf{a}_1^{(\mathrm{rx})} \mathbf{a}_1^{(\mathrm{irs})\mathrm{T}} \mathrm{diag}_k\left(\mathbf{S}^{(1)}\right) \mathbf{b}_1^{(\mathrm{irs})} \mathbf{b}_1^{(\mathrm{tx})\mathrm{T}} \mathbf{x}_k\right), \\
&= \gamma_1 \left(\mathbf{x}_k^{\mathrm{T}} \otimes \mathbf{I}_{M_r}\right) \mathrm{vec}\left(\mathbf{a}_1^{(\mathrm{rx})} \mathbf{a}_1^{(\mathrm{irs})\mathrm{T}} \mathrm{diag}_k\left(\mathbf{S}^{(1)}\right) \mathbf{b}_1^{(\mathrm{irs})} \mathbf{b}_1^{(\mathrm{tx})\mathrm{T}}\right), \\
&= \gamma_1 \left(\mathbf{x}_k^{\mathrm{T}} \otimes \mathbf{I}_{M_r}\right) \left((\mathbf{b}_1^{(\mathrm{irs})} \mathbf{b}_1^{(\mathrm{tx})\mathrm{T}})^{\mathrm{T}} \diamond (\mathbf{a}_1^{(\mathrm{rx})} \mathbf{a}_1^{(\mathrm{irs})\mathrm{T}})\right) \mathbf{s}_k^{(1)}, \\
&= \gamma_1 \left(\mathbf{s}_k^{(1)\mathrm{T}} \otimes \mathbf{x}_k^{\mathrm{T}} \otimes \mathbf{I}_{M_r}\right) \mathrm{vec}\left(\gamma_1 (\mathbf{b}_1^{(\mathrm{irs})} \mathbf{b}_1^{(\mathrm{tx})\mathrm{T}})^{\mathrm{T}} \diamond (\mathbf{a}_1^{(\mathrm{rx})} \mathbf{a}_1^{(\mathrm{irs})\mathrm{T}})\right), \\
&= \left(\mathbf{s}_k^{(1)\mathrm{T}} \otimes \mathbf{x}_k^{\mathrm{T}} \otimes \mathbf{I}_{M_r}\right) \mathrm{vec}\left(\gamma_1 (\mathbf{b}_1^{(\mathrm{tx})} \otimes \mathbf{a}_1^{(\mathrm{rx})})(\mathbf{b}_1^{(\mathrm{irs})\mathrm{T}} \diamond \mathbf{a}_1^{(\mathrm{irs})\mathrm{T}})\right), \\
&= \left(\mathbf{s}_k^{(1)\mathrm{T}} \otimes \mathbf{x}_k^{\mathrm{T}} \otimes \mathbf{I}_{M_r}\right) \mathbf{z}^{(1)} \in \mathbb{C}^{M_r \times 1}.
\end{aligned} \tag{3.11}$$

Stacking the K vectors associated to the first block, $\mathbf{y}_1^{(1)}, \ldots, \mathbf{y}_K^{(1)}$, in a row-wise fashion, we have

$$\begin{aligned}
\overline{\mathbf{y}}_1 &= \begin{bmatrix} \mathbf{y}_1^{(1)} \\ \vdots \\ \mathbf{y}_K^{(1)} \end{bmatrix}, \\
&= \begin{bmatrix} (\mathbf{s}_1^{(1)\mathrm{T}} \otimes \mathbf{x}_1^{\mathrm{T}} \otimes \mathbf{I}_{M_r}) \mathbf{z}^{(1)} \\ \vdots \\ (\mathbf{s}_K^{(1)\mathrm{T}} \otimes \mathbf{x}_K^{\mathrm{T}} \otimes \mathbf{I}_{M_r}) \mathbf{z}^{(1)} \end{bmatrix}, \\
&= \left[(\mathbf{S} \diamond \mathbf{X}) \otimes \mathbf{I}_{M_r}\right] \mathbf{z}^{(1)}, \\
&= \mathbf{C} \mathbf{z}^{(1)} \in \mathbb{C}^{M_r K \times 1}.
\end{aligned} \tag{3.12}$$

[2] In the literature, most of the IRSs are built with resonant circuits in order to reflect the impinging electromagnetic waves to a specified direction (ABEYWICKRAMA et al., 2020). However, in these circuits, the reflecting coefficient β usually varies within 0.2 (0 degree phase-shift) up to 1 (π or $-\pi$ phase-shift) (ABEYWICKRAMA et al., 2020). Nevertheless, the work of (BADLOE et al., 2017), shows that metamaterials are capable of perfectly absorbing the electromagnetic waves and reflect them to a specific direction at THz frequencies.

[3] In (JENSEN; DE CARVALHO, 2020) it is demonstrate that the optimal IRS's activation/initialization pattern follow the rows of a DFT.

Adding the noise term back, we have

$$\overline{\mathbf{y}}_1 = \mathbf{C}_{\text{PA}}\mathbf{z}^{(1)} + \mathbf{v}^{(1)} \in \mathbb{C}^{M_r K \times 1}, \tag{3.13}$$

where $\mathbf{v}^{(1)} = [\mathbf{v}_1^{(1)}, \ldots, \mathbf{v}_K^{(1)}]$, $\mathbf{C}_{\text{PA}} = [(\mathbf{S} \diamond \mathbf{X}) \otimes \mathbf{I}_{M_r}] \in \mathbb{C}^{M_r K \times M_r M_t N}$ is a semi-unitary matrix[4] containing the known system parameters, such as the pre-defined phase-shift matrix $\mathbf{S}$ (truncated DFT matrix) and $\mathbf{X} \in \mathbb{C}^{M_t \times K}$ (the pilot signal matrix). On the other hand, $\mathbf{z}^{(1)} = \gamma_1 \text{vec}\left((\mathbf{b}^{(\text{tx})} \otimes \mathbf{a}^{(\text{rx})})(\mathbf{b}_1^{(\text{irs})\text{T}} \diamond \mathbf{a}_1^{(\text{irs})\text{T}})\right)$ is the parameter vector to be estimated, which combines the channel gains and the array steering vectors from the TX, RX, and the IRS. A Least Squares (LS) estimate of $\mathbf{z}^{(1)}$ can be obtained from Equation (3.13) as

$$\hat{\mathbf{z}}^{(1)} \approx \mathbf{C}_{\text{PA}}^{\text{H}} \overline{\mathbf{y}}_1 \in \mathbb{C}^{M_r M_t N \times 1}. \tag{3.14}$$

It is important to note that, to ensure $\mathbf{C}_{\text{PA}}$ is left-invertible, we need to satisfy the condition $K \geq N M_t$. Defining $\hat{\mathbf{Z}}^{(1)} = \text{unvec}_{M_r M_t \times N}\left(\hat{\mathbf{z}}^{(1)}\right)$, we have

$$\begin{aligned} \hat{\mathbf{Z}}^{(1)} &\approx \gamma_1 (\mathbf{b}_1^{(\text{tx})} \otimes \mathbf{a}_1^{(\text{rx})})(\mathbf{b}_1^{(\text{irs})\text{T}} \diamond \mathbf{a}_1^{(\text{irs})\text{T}}), \\ &= \mathbf{f}_1 \mathbf{r}_1^{\text{T}} \in \mathbb{C}^{M_r M_t \times N}. \end{aligned} \tag{3.15}$$

Note that $\hat{\mathbf{Z}}^{(1)}$ is approximately a rank-one matrix, thus, defining $\hat{\mathbf{Z}}^{(1)} = \mathbf{U}^{(1)}\mathbf{\Sigma}^{(1)}\mathbf{V}^{(1)\text{H}}$ as the SVD of $\hat{\mathbf{Z}}^{(1)}$, we can obtain estimates of $\mathbf{f}_1$ and $\mathbf{r}_1$ from its dominant left and right singular vectors, respectively

$$\hat{\mathbf{f}}_1 = \mathbf{U}_1^{(1)} \in \mathbb{C}^{M_r M_t \times 1}, \tag{3.16}$$

$$\hat{\mathbf{r}}_1 = \mathbf{V}_1^{(1)*} \in \mathbb{C}^{N \times 1}. \tag{3.17}$$

Since $\hat{\mathbf{r}}_1$ is related to the arriving, $\mathbf{b}^{(\text{irs})}$, and departure, $\mathbf{a}^{(\text{irs})}$, array steering vectors from the first IRS, the optimum phase-shift of the first IRS are obtained as in Equation (2.24)

$$\mathbf{s}_{\text{opt}}^{(1)} = e^{-j\angle \hat{\mathbf{r}}_1} \in \mathbb{C}^{N \times 1}. \tag{3.18}$$

From $\hat{\mathbf{f}}_1$, we can obtain an estimate of the first column of the steering matrices $\mathbf{A}^{(\text{rx})}$ and $\mathbf{B}^{(\text{tx})}$ since $\hat{\mathbf{f}}_1 \approx \mathbf{b}_1^{(\text{tx})} \otimes \mathbf{a}_1^{(\text{rx})} \in \mathbb{C}^{M_r M_t \times 1}$. To this end, defining $\hat{\mathbf{F}}_1 = \text{unvec}_{Mr \times M_t}\left(\hat{\mathbf{f}}_1\right)$ yields

$$\hat{\mathbf{F}}_1 \approx \mathbf{a}_1^{(\text{rx})} \cdot \mathbf{b}_1^{(\text{tx})\text{T}}.$$

[4] Meaning that $\mathbf{C}_{\text{PA}}^{\text{H}}\mathbf{C}_{\text{PA}} = \mathbf{I}_{M_r M_t N}$ for the scenario where the interfering IRSs acts like Perfect Absorbers (PA).

Computing the SVD of $\hat{\mathbf{F}}_1 = \mathbf{U}^{\mathrm{f}(1)}\mathbf{\Sigma}^{\mathrm{f}(1)}\mathbf{V}^{\mathrm{f}(1)\mathrm{H}}$, the estimates of $\mathbf{a}_1^{(\mathrm{rx})}$ and $\mathbf{b}^{(\mathrm{tx})}$ are obtained, respectively, as

$$\hat{\mathbf{a}}_1^{(\mathrm{rx})} = \mathbf{u}_1^{\mathrm{f}(1)} \in \mathbb{C}^{M_r \times 1}, \tag{3.19}$$

$$\hat{\mathbf{b}}_1^{(\mathrm{tx})} = \mathbf{v}_1^{\mathrm{f}(1)*} \in \mathbb{C}^{M_t \times 1}. \tag{3.20}$$

After repeating the procedure from Equations (3.14) to (3.20) for all P blocks, the estimated transmit and receive steering matrices the TX and RX, respectively, are built as

$$\hat{\mathbf{A}}^{(\mathrm{rx})} = \left[\hat{\mathbf{a}}_1^{(\mathrm{rx})}, \ldots, \hat{\mathbf{a}}_P^{(\mathrm{rx})}\right] \in \mathbb{C}^{M_r \times P}, \tag{3.21}$$

$$\hat{\mathbf{B}}^{(\mathrm{tx})} = \left[\hat{\mathbf{b}}_1^{(\mathrm{tx})}, \ldots, \hat{\mathbf{b}}_P^{(\mathrm{tx})}\right] \in \mathbb{C}^{M_t \times P}. \tag{3.22}$$

Therefore, the total training overhead is given by $K \cdot P$ symbol periods, or, considering the minimum value of K, we have $N \cdot M_t \cdot P$ symbol periods. The path loss from the link TX - first IRS - RX is estimated from Equation (3.15) as

$$\hat{\gamma_1} = \mathbb{E}\{\hat{\mathbf{z}^{(1)}} \oslash \mathrm{vec}(\hat{\mathbf{f}}_1 \hat{\mathbf{r}}_1^{\mathrm{T}})\}. \tag{3.23}$$

Where $\mathbb{E}\{\cdot\}$ and $\oslash$ operators represents the expected value and the element-wise division, respectively.

3.2.2 IRS Interfering Signals Treatment

Because the previously case is based on the premise that the IRS is a perfect absorber it is necessary to obtain an estimation procedure that does not depend on this premise once this may not be the case in reality, due to hardware constraints, since the IRS still reflects part of the impinging signals. In this section, we consider once more the training sequence protocol shown in Figure 3.2. Let us start from equation (3.6) and rewrite it as

$$\begin{aligned}\mathbf{y}_k^{(1)} &= \gamma_1 \mathbf{a}_1^{(\mathrm{rx})} \mathbf{a}_1^{(\mathrm{irs})\mathrm{T}} \mathrm{diag}_k\left(\mathbf{S}^{(1)}\right) \mathbf{b}_1^{(\mathrm{irs})} \mathbf{b}_1^{(\mathrm{tx})\mathrm{T}} \mathbf{x}_k \\ &\quad + \underbrace{\sum_{p=2}^{P} \gamma_p \mathbf{a}_p^{(\mathrm{rx})} \mathbf{a}_p^{(\mathrm{irs})\mathrm{T}} \mathrm{diag}_k\left(\mathbf{S}^{(p)}\right) \mathbf{b}_p^{(\mathrm{irs})} \mathbf{b}_p^{(\mathrm{tx})\mathrm{T}} \mathbf{x}_k}_{\text{interference}} + \mathbf{v}_k^{(1)}, \\ &= \left(\gamma_1 \mathbf{a}_1^{(\mathrm{rx})} \mathbf{a}_1^{(\mathrm{irs})\mathrm{T}} \mathrm{diag}_k\left(\mathbf{S}^{(1)}\right) \mathbf{b}_1^{(\mathrm{irs})} \mathbf{b}_1^{(\mathrm{tx})\mathrm{T}} + \sum_{p=2}^{P} \gamma_p \mathbf{a}_p^{(\mathrm{rx})} \mathbf{a}_p^{(\mathrm{irs})\mathrm{T}} \mathrm{diag}_k\left(\mathbf{S}^{(p)}\right) \mathbf{b}_p^{(\mathrm{irs})} \mathbf{b}_p^{(\mathrm{tx})\mathrm{T}}\right) \mathbf{x}_k \\ &\quad + \mathbf{v}_k^{(1)} \in \mathbb{C}^{M_r \times 1}. \end{aligned} \tag{3.24}$$

Let us assume that, in the first block (P=1), the desired signal is coming from the first IRS, i.e., the signal reflected by the pth IRS, $\forall p \in \{2, \cdots, P\}$, is considered to be an interference. However, this time we will consider that the remaining IRSs are working as a regular scatter[5] instead of a perfect absorber. By neglecting the noise term, and applying properties (2.5), (2.6),(2.7) and (2.8) to Equation (3.24), we will obtain the expression

$$\begin{aligned}\mathbf{y}_k^{(1)} &= \mathbf{I}_{M_r} \left(\gamma_1 \mathbf{a}_1^{(\mathrm{rx})} \mathbf{a}_1^{(\mathrm{irs})\mathrm{T}} \mathrm{diag}_k\left(\mathbf{S}^{(1)}\right) \mathbf{b}_1^{(\mathrm{irs})} \mathbf{b}_1^{(\mathrm{tx})\mathrm{T}} + \sum_{p=2}^{P} \gamma_p \mathbf{a}_p^{(\mathrm{rx})} \mathbf{a}_p^{(\mathrm{irs})\mathrm{T}} \mathrm{diag}_k\left(\mathbf{S}^{(p)}\right) \mathbf{b}_p^{(\mathrm{irs})} \mathbf{b}_p^{(\mathrm{tx})\mathrm{T}}\right) \mathbf{x}_k, \\ &= \mathrm{vec}\left(\mathbf{I}_{M_r} \left(\gamma_1 \mathbf{a}_1^{(\mathrm{rx})} \mathbf{a}_1^{(\mathrm{irs})\mathrm{T}} \mathrm{diag}_k\left(\mathbf{S}^{(1)}\right) \mathbf{b}_1^{(\mathrm{irs})} \mathbf{b}_1^{(\mathrm{tx})\mathrm{T}} + \sum_{p=2}^{P} \gamma_p \mathbf{a}_p^{(\mathrm{rx})} \mathbf{a}_p^{(\mathrm{irs})\mathrm{T}} \mathrm{diag}_k\left(\mathbf{S}^{(p)}\right) \mathbf{b}_p^{(\mathrm{irs})} \mathbf{b}_p^{(\mathrm{tx})\mathrm{T}}\right) \mathbf{x}_k\right), \\ &= \left(\mathbf{x}_k^{\mathrm{T}} \otimes \mathbf{I}_{M_r}\right) \mathrm{vec}\left(\gamma_1 \mathbf{a}_1^{(\mathrm{rx})} \mathbf{a}_1^{(\mathrm{irs})\mathrm{T}} \mathrm{diag}_k\left(\mathbf{S}^{(1)}\right) \mathbf{b}_1^{(\mathrm{irs})} \mathbf{b}_1^{(\mathrm{tx})\mathrm{T}} + \sum_{p=2}^{P} \gamma_p \mathbf{a}_p^{(\mathrm{rx})} \mathbf{a}_p^{(\mathrm{irs})\mathrm{T}} \mathrm{diag}_k\left(\mathbf{S}^{(p)}\right) \mathbf{b}_p^{(\mathrm{irs})} \mathbf{b}_p^{(\mathrm{tx})\mathrm{T}}\right), \\ &= \mathbf{M}_k \left[\gamma_1 \left(\left(\mathbf{b}_1^{(\mathrm{irs})} \mathbf{b}_1^{(\mathrm{tx})\mathrm{T}}\right)^{\mathrm{T}} \diamond \left(\mathbf{a}_1^{(\mathrm{rx})} \mathbf{a}_1^{(\mathrm{irs})\mathrm{T}}\right)\right) \mathbf{s}_k^{(1)} + \mathrm{vec}\left(\sum_{p=2}^{P} \gamma_p \mathbf{a}_p^{(\mathrm{rx})} \mathbf{a}_p^{(\mathrm{irs})\mathrm{T}} \mathrm{diag}_k\left(\mathbf{S}^{(p)}\right) \mathbf{b}_p^{(\mathrm{irs})} \mathbf{b}_p^{(\mathrm{tx})\mathrm{T}}\right)\right], \\ &= \mathbf{M}_k \left[\gamma_1 \left(\left(\mathbf{b}_1^{(\mathrm{irs})} \mathbf{b}_1^{(\mathrm{tx})\mathrm{T}}\right)^{\mathrm{T}} \diamond \left(\mathbf{a}_1^{(\mathrm{rx})} \mathbf{a}_1^{(\mathrm{irs})\mathrm{T}}\right)\right) \mathbf{s}_k^{(1)} + \mathrm{vec}(\mathbf{H}^{(1)})\right] \in \mathbb{C}^{M_r \times 1}, \end{aligned} \tag{3.25}$$

where $\mathbf{M}_k = \left(\mathbf{x}_k^{\mathrm{T}} \otimes \mathbf{I}_{M_r}\right)$ and $\mathbf{H}^{(1)} = \sum_{p=2}^{P} \gamma_p \mathbf{a}_p^{(\mathrm{rx})} \mathbf{a}_p^{(\mathrm{irs})\mathrm{T}} \mathrm{diag}_k\left(\mathbf{S}^{(p)}\right) \mathbf{b}_p^{(\mathrm{irs})} \mathbf{b}_p^{(\mathrm{tx})\mathrm{T}}$ is the interference part for the first block. Since $\mathrm{vec}(\mathbf{H}^{(1)})$ remains constant across a block P we can use this to cancel the IRS interference. By subtracting the received signal vector at the $(k+1)$th time slot with the one at the time slot k, we have

[5] This is equivalent to set all the reflective coefficients $\beta_{n,k}^{(p)}$ to one for every interfering IRS. This way the IRS will reflect the signal without the active or passive beamforming.

$$\overline{\mathbf{y}}_{\overline{k}}^{(1)} = \mathbf{M}_{k+1}\left[\gamma_1\left((\mathbf{b}_1^{(\mathrm{irs})}\mathbf{b}_1^{(\mathrm{tx})\mathrm{T}})^{\mathrm{T}} \diamond (\mathbf{a}_1^{(\mathrm{rx})}\mathbf{a}_1^{(\mathrm{irs})\mathrm{T}})\right)\mathbf{s}_{k+1}^{(1)} + \mathrm{vec}(\mathbf{H}^{(1)})\right] - \mathbf{M}_k\left[\left((\gamma_1\mathbf{b}_1^{(\mathrm{irs})}\mathbf{b}_1^{(\mathrm{tx})\mathrm{T}})^{\mathrm{T}} \diamond (\mathbf{a}_1^{(\mathrm{rx})}\mathbf{a}_1^{(\mathrm{irs})\mathrm{T}})\right)\mathbf{s}_k^{(1)} + \mathrm{vec}(\mathbf{H}^{(1)})\right] \in \mathbb{C}^{M_r\times 1}. \tag{3.26}$$

Where $\overline{K} = K - 1$ and $\overline{\mathbf{y}}_{\overline{k}}^{(1)} = \mathbf{y}_{k+1}^{(1)} - \mathbf{y}_k^{(1)}$. Looking at Equation (3.26) we can see that to cancel the interference from $\mathrm{vec}(\mathbf{H}^{(1)})$ we have to obtain $\mathbf{M}_{k+1} = \mathbf{M}_k$. This is easily attainable if we guarantee that all pilots over the first block are the same for each K. This way if we have $\mathbf{M} = \mathbf{M}_1 = \cdots = \mathbf{M}_K$ then we can rewrite Equation (3.26) as

$$\begin{aligned}\overline{\mathbf{y}}_{\overline{k}}^{(1)} &= \mathbf{M}\left[\gamma_1\left((\mathbf{b}_1^{(\mathrm{irs})}\mathbf{b}_1^{(\mathrm{tx})\mathrm{T}})^{\mathrm{T}} \diamond (\mathbf{a}_1^{(\mathrm{rx})}\mathbf{a}_1^{(\mathrm{irs})\mathrm{T}})\right)\mathbf{s}_{k+1}^{(1)} + \mathrm{vec}(\mathbf{H}^{(1)})\right], \\ &\quad - \mathbf{M}\left[\gamma_1\left((\mathbf{b}_1^{(\mathrm{irs})}\mathbf{b}_1^{(\mathrm{tx})\mathrm{T}})^{\mathrm{T}} \diamond (\mathbf{a}_1^{(\mathrm{rx})}\mathbf{a}_1^{(\mathrm{irs})\mathrm{T}})\right)\mathbf{s}_k^{(1)} + \mathrm{vec}(\mathbf{H}^{(1)})\right], \\ &= \mathbf{M}\left(\gamma_1(\mathbf{b}_1^{(\mathrm{irs})}\mathbf{b}_1^{(\mathrm{tx})\mathrm{T}})^{\mathrm{T}} \diamond (\mathbf{a}_1^{(\mathrm{rx})}\mathbf{a}_1^{(\mathrm{irs})\mathrm{T}})\right)\left(\mathbf{s}_{k+1}^{(1)} - \mathbf{s}_k^{(1)}\right) + \mathbf{M}(\mathrm{vec}(\mathbf{H}^{(1)}) - \mathrm{vec}(\mathbf{H}^{(1)})), \\ &= \mathbf{M}\left(\gamma_1(\mathbf{b}_1^{(\mathrm{irs})}\mathbf{b}_1^{(\mathrm{tx})\mathrm{T}})^{\mathrm{T}} \diamond (\mathbf{a}_1^{(\mathrm{rx})}\mathbf{a}_1^{(\mathrm{irs})\mathrm{T}})\right)\mathbf{w}_{\overline{k}} \in \mathbb{C}^{M_r\times 1},\end{aligned} \tag{3.27}$$

where $\mathbf{w}_{\overline{k}} = \left(\mathbf{s}_{k+1}^{(1)} - \mathbf{s}_k^{(1)}\right)$. Now that we have our expression free from interference we can continue the process by applying properties (2.5),(2.6) and (2.7) to Equation (3.27), we obtain a expression similar to the Equation (3.11)

$$\begin{aligned}\overline{\mathbf{y}}_{\overline{k}}^{(1)} &= \gamma_1\left(\mathbf{w}_{\overline{k}} \otimes \mathbf{M}\right)\mathrm{vec}\left((\mathbf{b}_1^{(\mathrm{irs})}\mathbf{b}_1^{(\mathrm{tx})\mathrm{T}})^{\mathrm{T}} \diamond (\mathbf{a}_1^{(\mathrm{rx})}\mathbf{a}_1^{(\mathrm{irs})\mathrm{T}})\right), \\ &= \gamma_1\left(\mathbf{w}_{\overline{k}} \otimes \mathbf{M}\right)\mathrm{vec}\left((\mathbf{b}_1^{(\mathrm{tx})} \otimes \mathbf{a}_1^{(\mathrm{rx})})(\mathbf{b}_1^{(\mathrm{irs})\mathrm{T}} \diamond \mathbf{a}_1^{(\mathrm{irs})\mathrm{T}})\right), \\ &= \left(\mathbf{w}_{\overline{k}} \otimes \mathbf{M}\right)\mathbf{z}^{(1)} \in \mathbb{C}^{M_r\times 1}.\end{aligned} \tag{3.28}$$

Stacking the $\overline{K}$ vectors associated with the first block, $\overline{\mathbf{y}}_1^{(1)}, \cdots, \overline{\mathbf{y}}_{\overline{K}}^{(1)}$, in a row-wise fashion we have

$$\begin{aligned}\overline{\mathbf{y}}_1 &= \begin{bmatrix}\left(\mathbf{y}_2^{(1)} - \mathbf{y}_1^{(1)}\right) \\ \vdots \\ \left(\mathbf{y}_K^{(1)} - \mathbf{y}_{K-1}^{(1)}\right)\end{bmatrix}, \\ &= \begin{bmatrix}\left(\mathbf{w}_{\overline{1}} \otimes \mathbf{M}\right)\mathbf{z}^{(1)} \\ \vdots \\ \left(\mathbf{w}_{\overline{K}} \otimes \mathbf{M}\right)\mathbf{z}^{(1)}\end{bmatrix}, \\ &= \left(\mathbf{W}^{(1)} \otimes \mathbf{M}\right)\mathbf{z}^{(1)} \in \mathbb{C}^{M_r\overline{K}\times 1},\end{aligned} \tag{3.29}$$

where $\mathbf{W}^{(1)}$ is the matrix

$$\mathbf{W}^{(1)} = \begin{bmatrix} | & | & & | \\ \mathbf{s}_2^{(1)} - \mathbf{s}_1^{(1)} & \mathbf{s}_3^{(1)} - \mathbf{s}_2^{(1)} & \cdots & \mathbf{s}_K^{(1)} - \mathbf{s}_{K-1}^{(1)} \\ | & | & & | \end{bmatrix} \in \mathbb{C}^{N \times \overline{K}}. \tag{3.30}$$

Adding the noise vector back, we will obtain the expression

$$\begin{aligned} \overline{\mathbf{y}}_1 &= \left(\mathbf{W}^{(1)} \otimes \mathbf{M}\right) \mathbf{z}^{(1)} + \mathbf{v}^{(1)}, \\ &= \mathbf{C}_{\mathrm{RS}} \mathbf{z}^{(1)} + \mathbf{v}^{(1)} \in \mathbb{C}^{M_r \overline{K} \times 1}, \end{aligned} \tag{3.31}$$

where $\mathbf{v}^{(1)} = \left[\mathbf{v}_1^{(1)}, \cdots, \mathbf{v}_{\overline{K}}^{(1)}\right]$ and $\mathbf{C}_{\mathrm{RS}} = \left(\mathbf{W}^{(1)} \otimes \mathbf{M}\right) \in \mathbb{C}^{\overline{K} M_r \times M_r M_t N}$ are the noise vector and the matrix containing the known system parameters for the scenario where the interfering IRSs acts like Regular Scatterers (RS), respectively. $\mathbf{M}$ contains the Kronecker product between the pilot signal matrix $\mathbf{X} \in \mathbb{C}^{M_t \times \overline{K}}$ and the identity matrix $\mathbf{I}_{M_r}$. $\mathbf{W}^{(1)} \in \mathbb{C}^{N \times \overline{K}}$ represents the combined phase-shift matrix in which its columns are formed by subtracting two consecutive columns of a truncated DFT matrix of size $N \times \overline{K}$, i.e., $\overline{K} = K - 1$ columns as in Equation (3.30). Similarly to the process in Section 3.2.1 we can obtain a LS estimation of $\mathbf{z}^{(1)}$ from Equation (3.31)

$$\hat{\mathbf{z}}^{(1)} \approx \mathbf{C}_{\mathrm{RS}}^{+} \overline{\mathbf{y}}_1 \in \mathbb{C}^{M_r M_t N \times 1}. \tag{3.32}$$

It is important to note that, to ensure $\mathbf{C}_{\mathrm{RS}}$ is left-invertible again, we need to satisfy the new condition $\overline{K} = K - 1 \geq N M_t$. The proposed channel estimation and beamforming design procedure are summarized in Algorithm 1 for both methods. The total training overhead is $(K-1) \cdot P$ symbol periods. From now on the procedure to obtain the design for joint beamforming will develop similarly to the procedure of Equation (3.14) to Equation (3.23) from Section 3.2.1.

3.3 Algorithm

Algorithm 1: Channel Estimation and Beamforming

for p = *1:P* **do**

Estimate $\mathbf{z}^{(p)}$ as

$$\hat{\mathbf{z}}^{(p)} = \mathbf{C}_{\mathrm{D}}^{+}\overline{\mathbf{y}}_p \in \mathbb{C}^{M_r M_t N \times 1},$$

where $\mathrm{D} \in \{\mathrm{PA}, \mathrm{RS}\}$ indicates the scenarios of Perfect Absorbers (PA) and Regular Scatterers (RS), respectively. Define $\hat{\mathbf{Z}}_p = \mathrm{unvec}_{M_r M_t \times N}\left(\hat{\mathbf{z}}^{(p)}\right)$ and compute the SVD as $\hat{\mathbf{Z}}_p = \mathbf{U}^{(p)}\mathbf{\Sigma}^{(p)}\mathbf{V}^{(p)\mathrm{H}}$ to obtain the estimates

$$\hat{\mathbf{f}}_p = \mathbf{u}_1^{(p)} \in \mathbb{C}^{M_r M_t \times 1},$$
$$\hat{\mathbf{r}}_p = \mathbf{v}_1^{(p)*} \in \mathbb{C}^{N \times 1},$$

Set the optimum phase-shifts for the pth IRS as

$$\mathbf{s}_{\mathrm{opt}}^{(p)} = e^{-j\angle\hat{\mathbf{r}}_p} \in \mathbb{C}^{N \times 1},$$

Define $\hat{\mathbf{F}}_p = \mathrm{unvec}_{M_r \times M_t}\left(\hat{\mathbf{f}}_p\right)$ and compute its SVD as $\hat{\mathbf{F}}_p = \mathbf{U}^{\mathrm{f}(p)}\mathbf{\Sigma}^{\mathrm{f}(p)}\mathbf{V}^{\mathrm{f}(p)\mathrm{H}}$. Obtain the estimates of the TX and RX steering vectors, and the path loss for the TX - pth IRS - RX link as

$$\hat{\mathbf{a}}_p^{(\mathrm{rx})} = \mathbf{u}_1^{\mathrm{f}(p)} \in \mathbb{C}^{M_r \times 1},$$
$$\hat{\mathbf{b}}_p^{(\mathrm{tx})} = \mathbf{v}_1^{\mathrm{f}(p)*} \in \mathbb{C}^{M_t \times 1},$$
$$\hat{\gamma_1} = \mathbb{E}\{\hat{\mathbf{z}^{(1)}} \oslash \mathrm{vec}(\hat{\mathbf{f}}_1\hat{\mathbf{r}}_1^{\mathrm{T}})\}.$$

end

return $\hat{\mathbf{A}}^{(\mathrm{rx})} = \left[\hat{\mathbf{a}}_1^{(\mathrm{rx})}, \ldots, \hat{\mathbf{a}}_P^{(\mathrm{rx})}\right]$, $\hat{\mathbf{B}}^{(\mathrm{tx})} = \left[\hat{\mathbf{b}}_1^{(\mathrm{tx})}, \ldots, \hat{\mathbf{b}}_P^{(\mathrm{tx})}\right]$, $\boldsymbol{\gamma} = [\gamma_1, \cdots, \gamma_P]$ and $\mathbf{s}_{\mathrm{opt}}$.

Define $\hat{\mathbf{H}} = \hat{\mathbf{A}}^{(\mathrm{rx})}\mathrm{diag}(\boldsymbol{\gamma})\hat{\mathbf{B}}^{(\mathrm{tx})\mathrm{T}} \in \mathbb{C}^{M_r \times M_t}$ and compute its SVD as $\mathbf{H} = \mathbf{U}\mathbf{\Sigma}\mathbf{V}^{\mathrm{H}}$. Obtain the active beamforming matrices at the transmitter and receiver as

$$\mathbf{W} = \mathbf{U} \in \mathbb{C}^{M_r \times P},$$
$$\mathbf{Q} = \mathbf{V} \in \mathbb{C}^{M_t \times P}.$$

Algorithm 1 describes the channel estimation and beamforming design for both proposed scenarios, i.e., considering IRS absorption (Section 3.2.1) and interference (Section 3.2.2). After the estimation phase described by Figure 3.2 the data transmission phase starts and the received signal is given by

$$\mathbf{y}^{(\mathrm{d})} = \mathbf{W}^{\mathrm{H}}\mathbf{A}^{\mathrm{rx}}\mathrm{diag}(\boldsymbol{\gamma})\mathrm{diag}(\boldsymbol{\mu})\mathbf{B}^{(\mathrm{tx})\mathrm{T}}\mathbf{Q}\mathbf{x}^{(\mathrm{d})} + \mathbf{W}^{\mathrm{H}}\mathbf{v}^{(\mathrm{d})} \in \mathbb{C}^{P \times 1}, \tag{3.33}$$

where $\mathbf{v}^{(\mathrm{d})} \sim \mathcal{CN}(0, \sigma_{\mathrm{d}}^2)$ is the AWGN at the receiver, $\boldsymbol{\gamma} = [\gamma_1, \ldots, \gamma_P]^{\mathrm{T}} \in \mathbb{C}^{P \times 1}$ is

the vector containing the path loss and fast-fading between the TX and RX, while $\boldsymbol{\mu} = [\mu_1, \ldots, \mu_P]^{\mathrm{T}} \in \mathbb{C}^{P\times 1}$ is the path gain provided by the IRSs, which can be written as

$$\boldsymbol{\mu} = \begin{bmatrix} \mathbf{a}_1^{(\mathrm{irs})\mathrm{T}} \mathrm{diag}\left(\mathbf{s}_{\mathrm{opt}}^{(1)}\right) \mathbf{b}_1^{(\mathrm{irs})} \\ \vdots \\ \mathbf{a}_P^{(\mathrm{irs})\mathrm{T}} \mathrm{diag}\left(\mathbf{s}_{\mathrm{opt}}^{(P)}\right) \mathbf{b}_P^{(\mathrm{irs})} \end{bmatrix} \in \mathbb{C}^{P\times 1}.$$

4 Numerical Analysis

In this section, we evaluate the performance of the proposed scenarios in terms of SE by comparing it with the one without the IRS. The transmitted symbols are normalized such that $\mathbb{E}\{\mathbf{x}^{(\mathrm{d})}\mathbf{x}^{(\mathrm{d})H}\} = 1$. The SNR is controlled by varying the noise power σ_{d}^2, i.e., SNR $= 1/\sigma_{\mathrm{d}}^2$. The AoA α_p and AoD β_p are randomly generated from an uniform distribution with values between $[-\pi, \pi]$. At the IRS, the elevation angles of departure and arrival are generated from an uniform distribution between $[-\pi/2, \pi/2]$. The combined effect of path-loss and fast-fading components is modeled as Gaussian random variables with $\gamma_p \sim \mathcal{CN}(0, 1)$. The pilot-assisted training sequence occur at SNR value of 25 dB. Considering the method in Section 3.2.2, the amplitude coefficient values used is $\beta_n = 1, \forall n \in \{1, \cdots, N\}$. The equivalent MIMO channel (including the transmit and receive beamformings) is given as

$$\mathbf{H}_{\mathrm{eq}} = \mathbf{W}^{\mathrm{H}}\mathbf{A}^{\mathrm{rx}}\mathrm{diag}(\lambda)\mathrm{diag}(\mu)\mathbf{B}^{(\mathrm{tx})\mathrm{T}}\mathbf{Q}. \tag{4.1}$$

The spectral efficiency is then calculated as

$$\mathrm{SE\ (bps/Hz)} = \log_2\left[\det\left(\mathbf{I}_P + \frac{\mathbf{H}_{\mathrm{eq}}\mathbf{R}_{xx}\mathbf{H}_{\mathrm{eq}}^{\mathrm{H}}}{\sigma_{\mathrm{d}}^2}\right)\right], \tag{4.2}$$

with $\mathbf{R}_{xx} = \mathbb{E}\{\mathbf{x}^{(\mathrm{d})}\mathbf{x}^{(\mathrm{d})H}\}$, and trace $\left(\mathbf{Q}\mathbf{R}_{xx}\mathbf{Q}^{\mathrm{H}}\right) = 1$. Two scenarios are considered in this chapter. The first, called as Perfect Absorbers (PA) and introduced in Section (3.2.1), the IRSs from different time blocks are in absorption mode, i.e., their amplitude coefficients are set to zero. While in the second scenario, the IRSs from different time blocks act like Regular Scatterers (RS), i.e., their amplitude coefficient are different from zero and thus an additional signal processing step is required at the receiver to mitigate this interference as explained in Section (3.2.2).

4.1 Discussion

In this section we discuss the performance of the IRS considering the scenarios of PA and RS. We analyse the impact of the number of IRSs, the number of IRS's reflective elements and the ideal strategy of IRSs deployment (centralized or decentralized) for the proposed scenario of multi-IRS aided MIMO systems.

4.1.1 Number of IRSs

Figure 4.1 Spectral efficiency for different values of P.

(a) PA Scenario.

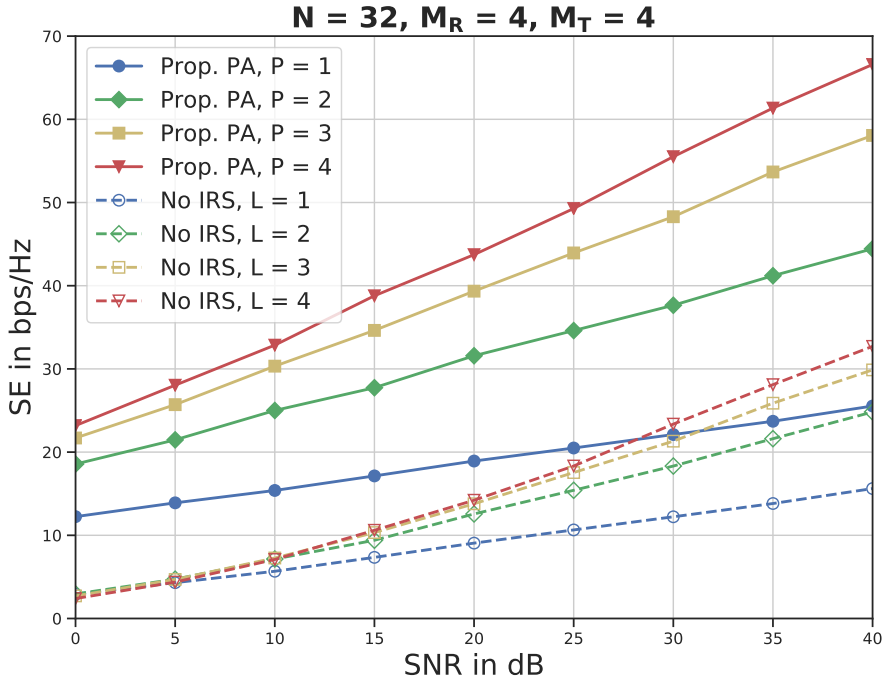

(b) RS Scenario.

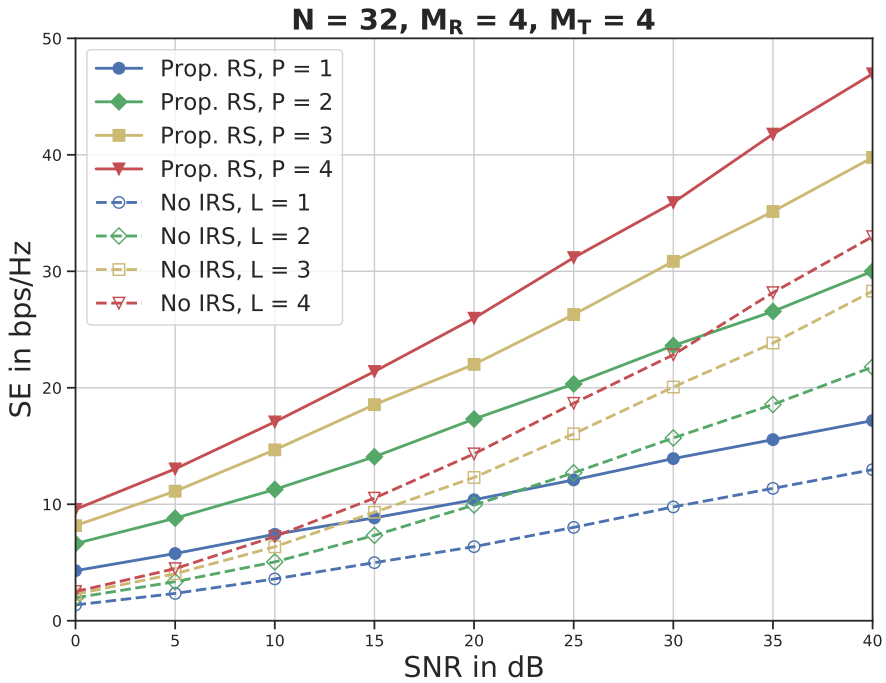

Source: Produced by the author.

Figure 4.2 PA *vs.* RS Scenarios: Spectral efficiency for different values of P.

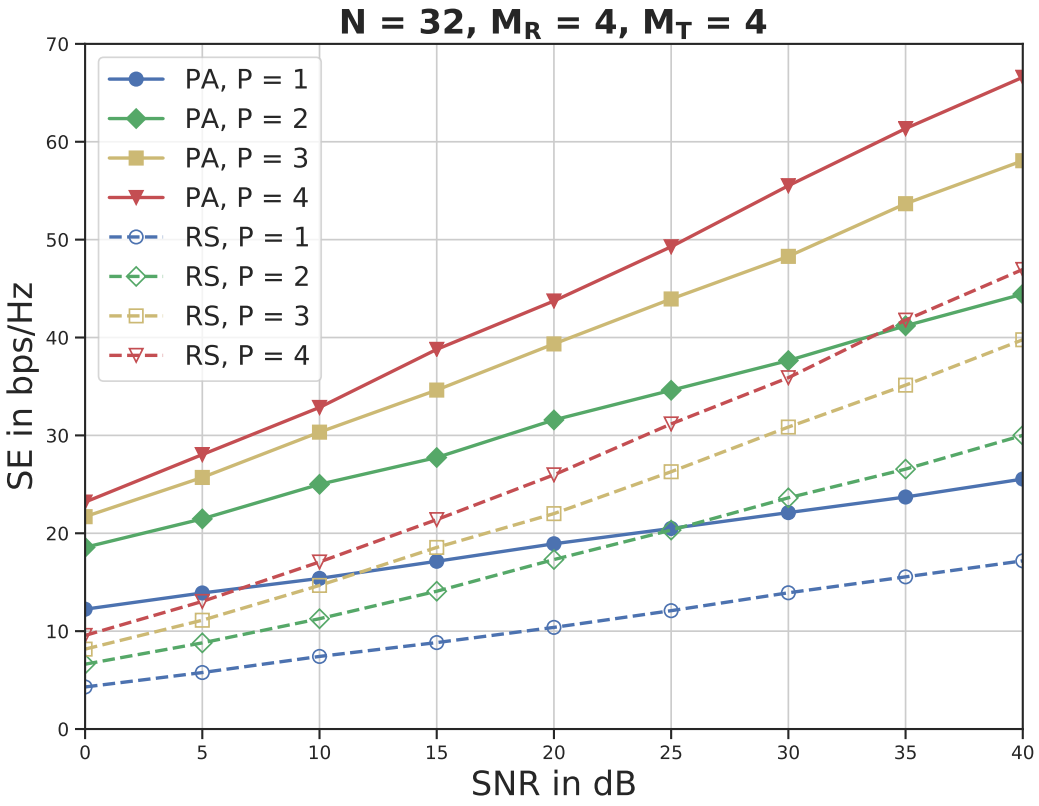

Source: Produced by the author.

In Figure 4.1a, we can observe the impact of deploying multiple IRSs in the considered MIMO communication system. When $P = 4$ and SNR is equal to 20 dB, the proposed multi-IRS scenario achieves an SE of 44 bps/Hz approximately, while for the one without IRS, the SE is approximately 14 bps/Hz. This is clear, since as P increases we have more IRSs in the system to perform a smart passive beamforming. However, it is important to note that, as P increases, the training overhead also increases since $K \cdot P$ is required. At high SNR values (> 30 dB), the single-IRS scenario ($P = 1$) is outperformed by the scenario without IRS.

In Figure 4.1b, we can observe the impact of deploying multiple IRSs. Considering that $P = 4$ and SNR is equal to 20 dB, the proposed multi-IRS scenario achieves an SE of 26 bps/Hz while in the previous scenario it was possible to achieve the value of 44 bps/Hz. This performance drop is expected since in Figure 4.1b, an interference canceling step is necessary with Equation (3.30). In this case we can perceive that at low SNR values (< 20 dB), the scenario with $P = 1$ is outperformed by the scenario without the aid of IRSs starting from SNR values of 10 dB. Meanwhile, the scenario with $P = 2$ is outperformed only at high SNR values (> 30 dB).

In Figure 4.2, we compare both scenarios directly. We observe that for $P = 2$ the scenario PA outperforms the scenario RS of $P = \{1, 2, 3, 4\}$ for almost all ranges of SNR. The results are expected, since in the scenario RS we have at Equation (3.32) the matrix $\mathbf{C}_{\text{RS}}$ multiplying the noise vector. Since the columns of this matrix are generated by

subtracting two consecutive columns of a truncated DFT matrix as in Equation (3.30), we will obtain a non-unitary matrix that will change the statistical properties of the noise vector. While in the scenario PA, $\mathbf{C}_{\mathrm{PA}}$ is a semi-unitary matrix and thus will not change the statistical properties of the noise vector in Equation (3.14).

4.1.2 Number of Reflective Elements

Figure 4.3 Spectral efficiency for N IRS elements.

(a) PA Scenario.

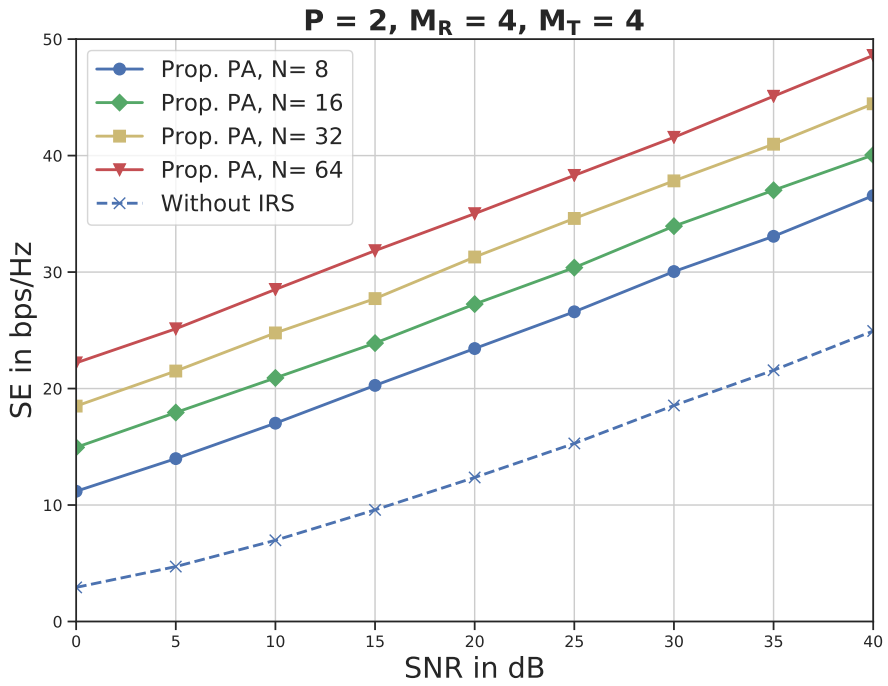

(b) RS Scenario.

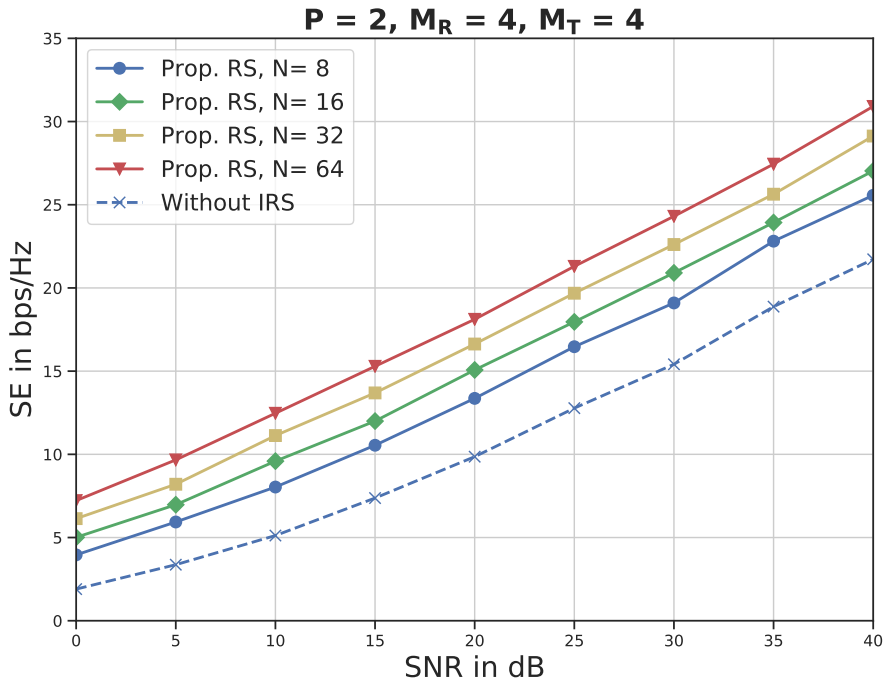

Source: Produced by the author.

Figure 4.4 PA *vs.* RS Scenarios: Spectral efficiency for N IRS elements.

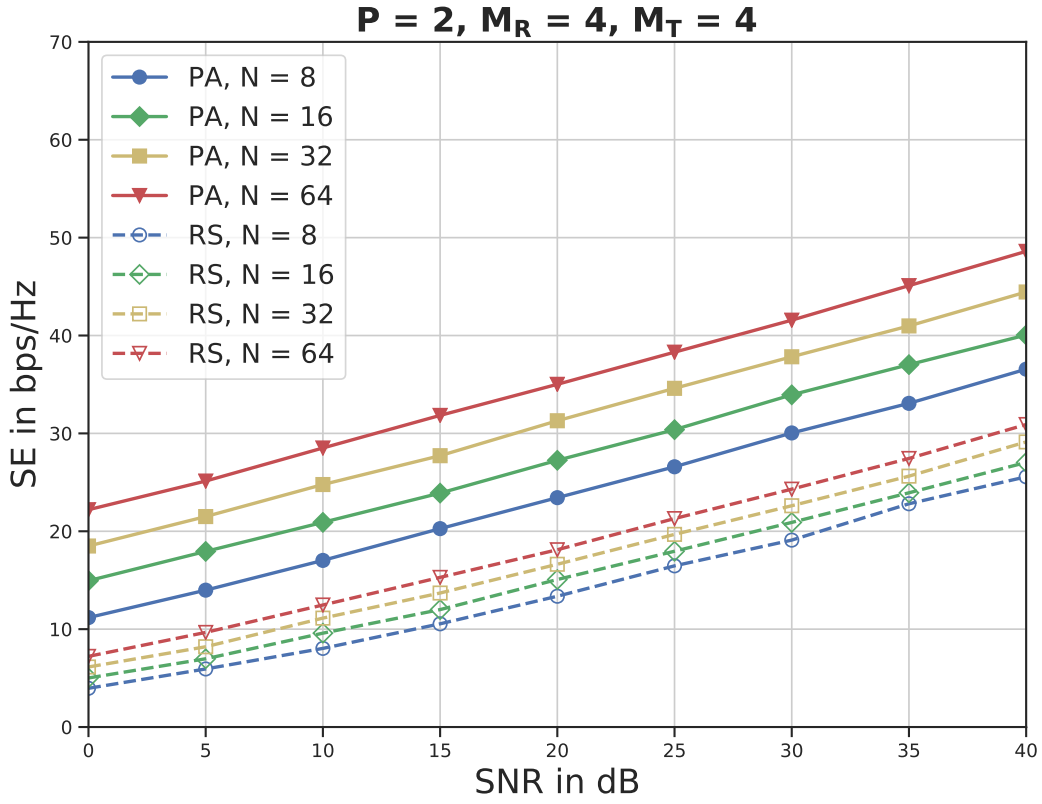

Source: Produced by the author.

In Figure 4.3a, we fix the number of IRSs as $P = 2$, while varying the number N of reflecting elements per IRS. As expected, the SE increases with the increase of N and it occurs in a linear fashion. As a reference for comparison, we also plot the SE for the case without IRS. We notice that, even for a small number of reflecting elements ($N = 8$), the proposed scenario outperforms the one without IRS. We also can observe that it seems to exist a direct relation between the scenario $N = 8$ and $N = 64$ as they are associated by the squared value. The case $N = 64$ has an SE that is approximately two times the SE from $N = 8$. This could be a hint of a behaviour inherent to the proposed scenario and could be potentially used to make approximations for scenarios with a high number of reflective elements.

In Figure 4.3b, we repeat the process the scenario RS. Once again, as expected, the scenarios with the aid of IRSs easily outperforms the scenarios without IRSs. Though, we can observe a degradation in the performance when compare with the scenario PA. However, we can see that the previously discussed relation between the cases $N = 8$ and $N = 64$ still holds truth.

In Figure 4.4, the scenario PA outperforms all the scenarios RS. Not only that, but we can notice that if our objective is to increase the SE the scenario RS seems to be less effective than the scenario PA when it comes to increase the number of reflective elements to achieve higher data rates.

4.1.3 Constant Transmission Rate

Figure 4.5 PA *vs.* RS Scenarios: Spectral efficiency for different values of N and P in order to ensure the same training overhead for all cases.

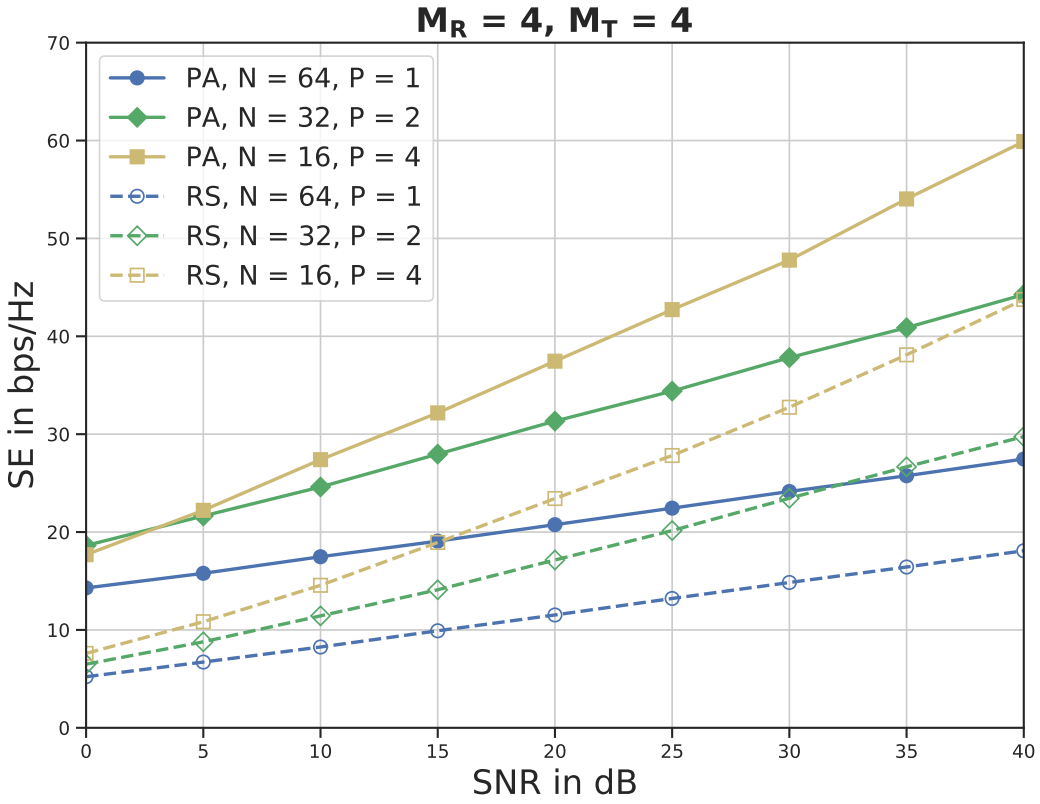

Source: Produced by the author.

In Figure 4.5, shows a SE comparison for the proposed scenarios of PA and RS with three different configurations that have the same training overhead, i.e., $K \cdot P$, that is equivalent to $N \cdot M_t \cdot P$.

Considering the scenario PA, we can observe that the setup with $N = 16$ and $P = 4$ has a better performance than the one with $N = 64$ and $P = 1$. This is an interesting result. One may conclude from that, in the proposed scenario, it is preferable to have P IRSs with N reflecting elements each, than a single IRS with $P \cdot N$ elements, in order to enjoy the diversity present in the system. Meaning that a strategy of decentralized deployment is better than a centralized deployment.

The scenario RS, we can conclude that it is preferable to have P IRSs with N reflecting elements each, than a single IRS with $P \cdot N$ elements, for the same reasons of the previous scenario. Though, this behavior is present only at values of SNR > 10 dB, e.g., considering the value of SNR equal to 15 dB, we notice that the SE is approximately 10 bps/Hz for the scenario with $N = 64$ and $P = 1$ while the SE is approximately 20 bps/Hz for the scenario with $N = 16$ and $P = 4$. As expected, the scenario PA achieves better performance than the scenario RS. We notice that for the scenarios $N = 32$ and $P = 2$ and $N = 16$ and

$P = 4$ the RS scenario outperforms the scenario PA for the scenario $N = 64$ and $P = 1$ at high values of SNR (> 30 dB).

The comparisons between the scenarios PA and RS are necessary. Considering the current state-of-art metasurfaces (BADLOE et al., 2017), it is not feasible yet a metasurface acting like a perfect absorber because there is still some interferences of impinging electromagnetic waves (or even the self-interference of the reflective elements of the IRS) that could leak to the system and potentially deteriorate the overall performance. So, considering the current state of the metasurfaces technology, the scenario proposed in Section 3.2.1 is an ideal case. Meanwhile, the method proposed in Section 3.2.2 solve this problem by using an interference cancel procedure that subtracts two consecutive time-slotted signals.

5 Conclusion

In this work, we have proposed a channel estimation and joint beamforming design for a MIMO multi-IRS system, where multiple IRSs are placed on the exact location of the system scatterers. By separating the scatterers with the help of the IRSs, the channel is estimated and the active and passive beamformings are designed. Since each IRS is assumed to be individually aligned with a different scatterer, an optimum multipath diversity gain is efficiently exploited. We compare two scenarios: The first, called as Perfect Absorbers (PA), the IRSs from different time blocks are in absorption mode, i.e., their amplitude coefficient are set to zero. While in the second scenario, the IRSs from different time blocks act like normal Regular Scatterers (RS), i.e., their amplitude coefficient are different from zero and thus an additional signal processing step is required at the receiver to mitigate this interference. As expected, we notice that the performance of the proposed scenario increases linearly with the number of IRSs or the number of IRS's reflective elements. Finally, we compare different deployment strategies for multi-IRS systems, and we show that, in the proposed scenario, it is preferable to have more IRSs deployed with few elements, than only one IRS with a large number of reflective elements, for the same transmission rate.

As perspective, we investigate the case when the number of scatterers is larger than the possible number of IRSs deployment in the system. Also, we aim at considering a scenario where is possible to implement the coupling effect between the amplitude reflection and the phase-shift. Furthermore, phase-shift and amplitude quantization on multi-IRS aided MIMO systems is an interesting topic.

References

ABEYWICKRAMA, S.; ZHANG, R.; WU, Q.; YUEN, C. Intelligent reflecting surface: Practical phase shift model and beamforming optimization. *IEEE Transactions on Communications*, IEEE, v. 68, n. 9, p. 5849–5863, 2020.

ALEXANDROPOULOS, G. C.; VLACHOS, E. A hardware architecture for reconfigurable intelligent surfaces with minimal active elements for explicit channel estimation. In: IEEE. ICASSP 2020-2020 IEEE International Conference on Acoustics, Speech and Signal Processing (ICASSP). 2020. p. 9175–9179.

ARAÚJO, G. T. DE; DE ALMEIDA, A. L.; BOYER, R. Channel estimation for intelligent reflecting surface assisted MIMO systems: A tensor modeling approach. *IEEE Journal of Selected Topics in Signal Processing*, IEEE, v. 15, n. 3, p. 789–802, 2021.

ARDAH, K.; GHEREKHLOO, S.; ALMEIDA, A. L. DE; HAARDT, M. TRICE: A Channel Estimation Framework for RIS-Aided Millimeter-Wave MIMO Systems. *IEEE Signal Processing Letters*, IEEE, v. 28, p. 513–517, 2021.

BADLOE, T.; MUN, J.; RHO, J. Metasurfaces-based absorption and reflection control: perfect absorbers and reflectors. *Journal of Nanomaterials*, Hindawi, v. 2017, 2017.

BJÖRNSON, E.; ÖZDOGAN, Ö.; LARSSON, E. G. Intelligent reflecting surface versus decode-and-forward: How large surfaces are needed to beat relaying? *IEEE Wireless Communications Letters*, IEEE, v. 9, n. 2, p. 244–248, 2019.

BJÖRNSON, E.; ÖZDOGAN, Ö.; LARSSON, E. G. Reconfigurable intelligent surfaces: Three myths and two critical questions. *IEEE Communications Magazine*, IEEE, v. 58, n. 12, p. 90–96, 2020.

BUKHARI, S. S.; VARDAXOGLOU, J. Y.; WHITTOW, W. A metasurfaces review: Definitions and applications. *Applied Sciences*, Multidisciplinary Digital Publishing Institute, v. 9, n. 13, p. 2727, 2019.

CAVALCANTI, F.; MACIEL, T.; FREITAS, W.; SILVA, Y. *Comunicação móvel celular*. Elsevier, 2018. ISBN 9788535280432. Available from: <https://books.google.com.br/books?id=hnJgDwAAQBAJ>.

CUI, T. J.; QI, M. Q.; WAN, X.; ZHAO, J.; CHENG, Q. Coding metamaterials, digital metamaterials and programmable metamaterials. *Light: Science & Applications*, Nature Publishing Group, v. 3, n. 10, e218–e218, 2014.

DI RENZO, M.; NTONTIN, K.; SONG, J.; DANUFANE, F. H.; QIAN, X.; LAZARAKIS, F.; DE ROSNY, J.; PHAN-HUY, D.-T.; SIMEONE, O.; ZHANG, R., et al. Reconfigurable intelligent surfaces vs. relaying: Differences, similarities, and performance comparison. *IEEE Open Journal of the Communications Society*, IEEE, v. 1, p. 798–807, 2020.

FOO, S. Liquid-crystal reconfigurable metasurface reflectors. In: IEEE. 2017 IEEE International Symposium on Antennas and Propagation & USNC/URSI National Radio Science Meeting. 2017. p. 2069–2070.

GEIM, A. K.; NOVOSELOV, K. S. The rise of graphene. In: NANOSCIENCE and technology: a collection of reviews from nature journals. World Scientific, 2010. p. 11–19.

GOLDSMITH, A. *Wireless Communications*. Cambridge University Press, 2005. ISBN 9781139445849. Available from: <https://books.google.com.br/books?id=ZtFVAgAAQBAJ>.

GONG, S.; LU, X.; HOANG, D. T.; NIYATO, D.; SHU, L.; KIM, D. I.; LIANG, Y.-C. Toward Smart Wireless Communications via Intelligent Reflecting Surfaces: A Contemporary Survey. *IEEE Communications Surveys & Tutorials*, IEEE, v. 22, n. 4, p. 2283–2314, 2020.

HE, Z.-Q.; YUAN, X. Cascaded channel estimation for large intelligent metasurface assisted massive MIMO. *IEEE Wireless Communications Letters*, IEEE, v. 9, n. 2, p. 210–214, 2019.

JENSEN, T. L.; DE CARVALHO, E. An optimal channel estimation scheme for intelligent reflecting surfaces based on a minimum variance unbiased estimator. In: IEEE. ICASSP 2020-2020 IEEE International Conference on Acoustics, Speech and Signal Processing (ICASSP). 2020. p. 5000–5004.

LIASKOS, C.; NIE, S.; TSIOLIARIDOU, A.; PITSILLIDES, A.; IOANNIDIS, S.; AKYILDIZ, I. A new wireless communication paradigm through software-controlled metasurfaces. *IEEE Communications Magazine*, IEEE, v. 56, n. 9, p. 162–169, 2018.

MA, X.; CHEN, Z.; CHEN, W.; CHI, Y.; LI, Z.; HAN, C.; WEN, Q. Intelligent reflecting surface enhanced indoor terahertz communication systems. *Nano Communication Networks*, Elsevier, v. 24, p. 100284, 2020.

ÖZDOGAN, Ö.; BJÖRNSON, E.; LARSSON, E. G. Intelligent reflecting surfaces: Physics, propagation, and pathloss modeling. *IEEE Wireless Communications Letters*, IEEE, v. 9, n. 5, p. 581–585, 2019.

PAULRAJ, A.; ERINGEN, A.; ROHIT, A.; NABAR, R.; GORE, D.; PRESS, C. U. *Introduction to Space-Time Wireless Communications*. Cambridge University Press, 2003. ISBN 9780521826150. Available from: <https://books.google.com.br/books?id=YQSsoPDfyngC>.

SALMI, J.; RICHTER, A.; KOIVUNEN, V. Detection and tracking of MIMO propagation path parameters using state-space approach. *IEEE Transactions on Signal Processing*, IEEE, v. 57, n. 4, p. 1538–1550, 2008.

SHEN, H.; XU, W.; GONG, S.; HE, Z.; ZHAO, C. Secrecy rate maximization for intelligent reflecting surface assisted multi-antenna communications. *IEEE Communications Letters*, IEEE, v. 23, n. 9, p. 1488–1492, 2019.

TAHA, A.; ALRABEIAH, M.; ALKHATEEB, A. Enabling large intelligent surfaces with compressive sensing and deep learning. *IEEE Access*, IEEE, v. 9, p. 44304–44321, 2021.

TSE, D.; VISWANATH, P. *Fundamentals of Wireless Communication*. Cambridge University Press, 2005. (Wiley series in telecommunications). ISBN 9780521845274. Available from: <https://books.google.com.br/books?id=66XBb5tZX6EC>.

VAN TREES, H. *Optimum Array Processing*. Wiley-Interscience, 2001. ISBN 9781601193872. Available from: <https://books.google.com.br/books?id=BYPkswEACAAJ>.

WANG, P.; FANG, J.; YUAN, X.; CHEN, Z.; LI, H. Intelligent reflecting surface-assisted millimeter wave communications: Joint active and passive precoding design. *IEEE Transactions on Vehicular Technology*, IEEE, 2020.

WANG, Z.; LIU, L.; CUI, S. Channel estimation for intelligent reflecting surface assisted multiuser communications. In: IEEE. 2020 IEEE Wireless Communications and Networking Conference (WCNC). 2020. p. 1–6.

WEI, L.; HUANG, C.; ALEXANDROPOULOS, G. C.; YUEN, C.; ZHANG, Z.; DEBBAH, M. Channel estimation for RIS-empowered multi-user MISO wireless communications. *IEEE Transactions on Communications*, IEEE, 2021.

WU, Q.; ZHANG, R. Towards smart and reconfigurable environment: Intelligent reflecting surface aided wireless network. *IEEE Communications Magazine*, IEEE, v. 58, n. 1, p. 106–112, 2019.

WU, Q.; ZHANG, S.; ZHENG, B.; YOU, C.; ZHANG, R. Intelligent reflecting surface aided wireless communications: A tutorial. *IEEE Transactions on Communications*, IEEE, 2021.

YANG, Y.; ZHENG, B.; ZHANG, S.; ZHANG, R. Intelligent reflecting surface meets OFDM: Protocol design and rate maximization. *IEEE Transactions on Communications*, IEEE, v. 68, n. 7, p. 4522–4535, 2020.

YOU, C.; ZHANG, R. Wireless Communication Aided by Intelligent Reflecting Surface: Active or Passive? *arXiv preprint arXiv:2106.10963*, 2021.

ZAPPONE, A.; DI RENZO, M.; SHAMS, F.; QIAN, X.; DEBBAH, M. Overhead-aware design of reconfigurable intelligent surfaces in smart radio environments. *IEEE Transactions on Wireless Communications*, IEEE, 2020.